Inorganic Chemistry

Article

pubs.acs.org/IC

Syntheses, Structural, Magnetic, and Electron Paramagnetic Resonance Studies of Monobridged Cyanide and Azide Dinuclear Copper(II) Complexes: Antiferromagnetic Superexchange Interactions

Daniel L. Reger,*[,†] Andrea E. Pascui,[†] Mark D. Smith,[†] Julia Jezierska,[‡] and Andrew Ozarowski*[,§]

[†]Department of Chemistry and Biochemistry, University of South Carolina, Columbia, South Carolina 29208, United States

[‡]Faculty of Chemistry, University of Wrocław 50-383 Wrocław, Poland

[§]National High Magnetic Field Laboratory, Florida State University, Tallahassee, Florida 32310, United States

Supporting Information

ABSTRACT: The reactions of $Cu(ClO_4)_2$ with NaCN and the ditopic ligands *m*-bis[bis(1-pyrazolyl)methyl]benzene ($\mathbf{L}_m$) or *m*-bis[bis(3,5-dimethyl-1-pyrazolyl)methyl]benzene ($\mathbf{L}_m$*) yield $[Cu_2(\mu\text{-CN})(\mu\text{-}\mathbf{L}_m)_2](ClO_4)_3$ (**1**) and $[Cu_2(\mu\text{-CN})(\mu\text{-}\mathbf{L}_m\text{*})_2](ClO_4)_3$ (**3**). In both, the cyanide ligand is linearly bridged (μ-1,2) leading to a separation of the two copper(II) ions of ca. 5 Å. The geometry around copper(II) in these complexes is distorted trigonal bipyramidal with the cyanide group in an equatorial position. The reaction of $[Cu_2(\mu\text{-F})(\mu\text{-}\mathbf{L}_m)_2](ClO_4)_3$ and $(CH_3)_3SiN_3$ yields $[Cu_2(\mu\text{-N}_3)(\mu\text{-}\mathbf{L}_m)_2](ClO_4)_3$ (**2**), where the azide adopts end-on (μ-1,1) coordination with a Cu−N−Cu angle of 138.0° and a distorted square pyramidal geometry about the copper(II) ions. Similar chemistry in the more sterically hindered $\mathbf{L}_m$* system yielded only the coordination polymer $[Cu_2(\mu\text{-}\mathbf{L}_m\text{*})(\mu\text{-N}_3)_2(N_3)_2]$. Attempts to prepare a dinuclear complex with a bridging iodide yield the copper(I) complex $[Cu_5(\mu\text{-I}_4)(\mu\text{-}\mathbf{L}_m\text{*})_2]I_3$. The complexes **1** and **3** show strong antiferromagnetic coupling, $-J = 135$ and 161 cm^{-1}, respectively. Electron paramagnetic resonance (EPR) studies coupled with density functional theory (DFT) calculations show that the exchange interaction is transmitted through the d_{z^2} and the bridging ligand s and p_x orbitals. High field EPR studies confirmed the d_{z^2} ground state of the copper(II) ions. Single-crystal high-field EPR has been able to definitively show that the signs of *D* and *E* are positive. The zero-field splitting is dominated by the anisotropic exchange interactions. Complex **2** has $-J = 223$ cm^{-1} and DFT calculations indicate a predominantly $d_{x^2-y^2}$ ground state.

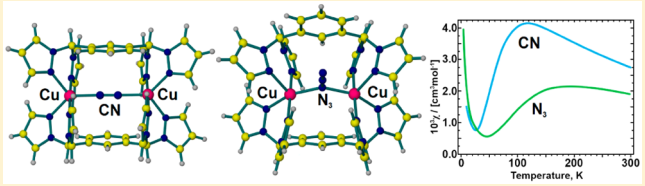

INTRODUCTION

Dinuclear copper(II) complexes bridged by a single anion can serve as model compounds for the treatment of superexchange interactions in more complicated systems.[1] We have previously reported the linearly bridged complexes of the type $[Cu_2(\mu\text{-X})(\mu\text{-}\mathbf{L}_m\text{*})_2](ClO_4)_3$ where X = F^-, Cl^-, OH^-, Br^- and $\mathbf{L}_m$* = *m*-bis[bis(3,5-dimethyl-1-pyrazolyl)methyl]benzene, Scheme 1, showing that this system supports extremely strong antiferromagnetic superexchange interactions, with $-J$ = 340, 720, 808, and 945 cm^{-1}, respectively ($\hat{\mathbf{H}} = -J\,\hat{\mathbf{S}}_1\hat{\mathbf{S}}_2$).[2] We[2b,c] and others[1d,h] have previously discussed extensively examples with X = F^- and OH^-.

This unusual $[Cu_2(\mu\text{-X})(\mu\text{-L}_m\text{*})_2](ClO_4)_3$ system, where the structure is held relatively constant, presents the first example of a synthetically available series of complexes that consistently promote the linear Cu−X−Cu (180°) bridging arrangement. Even though the theoretical basis for treating the antiferromagnetic interactions in dinuclear compounds is well developed,[3] the linear Cu−X−Cu arrangement is virtually unstudied prior to our work due to the lack of compounds of this type. In the $[Cu_2(\mu\text{-X})(\mu\text{-}\mathbf{L}_m\text{*})_2](ClO_4)_3$ series, the magnetic orbitals have predominantly d_{z^2} character, as a result of the pseudo Jahn−Teller distorted, axially compressed trigonal bipyramidal geometry around copper(II). The large $-J$ values, increasing from F^- to the Br^- in the halide bridged

Scheme 1. Schematic Representation of the Metallacycle $[Cu_2(\mu\text{-X})(\mu\text{-}\mathbf{L}_m\text{*})_2]^{3+}$

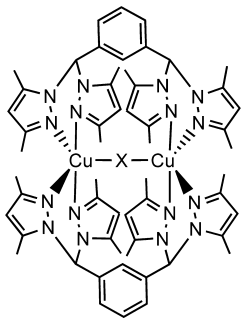

Received: October 10, 2014
Published: January 20, 2015

DOI: 10.1021/ic502485p
Inorg. Chem. 2015, 54, 1487−1500

series, are explained by increasingly stronger interaction between the valence p orbital of the bridging group with the "doughnut" portion of the d_{z^2} orbitals in the antibonding antisymmetric combination, than the interaction between the lower lying s orbital with d_{z^2} in the symmetric combination. Therefore, the energy of the antisymmetric orbital rises faster and the singlet state is stabilized. The very large $-J$ value for the OH^- bridged complex is a result of the unusually large overlap integral of the magnetic orbitals and the more efficient spin delocalization toward the p orbital in comparison to the fluoride bridged compound.

We report here the structure, magnetic, and electron paramagnetic resonance (EPR) properties of complexes containing more complex bridges, end-on (μ-1,1) N_3^- and end-to-end (μ-1,2) CN^- in similar metallacyclic compounds of $\mathbf{L}_m$, *m*-bis[bis(1-pyrazolyl)methyl]benzene, and $\mathbf{L}_m$*. Even though several dinuclear copper(II) compounds with doubly bridged N_3^- have been reported,[4] the number of compounds with a single end-on (μ-1,1) N_3^- exclusively mediating the superexchange interaction is limited,[5] and in these examples the Cu−N−Cu bridging angle is relatively low, ∼90−115°. The CN^- bridged dinuclear compounds are even less extensively studied as a result of the reducing character of this anion in the presence of copper(II).[6] We also describe the structure of the pentametallic copper(I) I^- bridged compound that was isolated in an attempt to synthesize the copper(II) dinuclear metallacycle with the large I^- ion as the bridging group; the reducing effect of iodide on copper(II) is well-known, and only a few successful attempts are documented where species with a copper(II)-iodide bond were isolated.[7]

EXPERIMENTAL SECTION

General Considerations. The syntheses of the compounds were carried out under nitrogen atmosphere using standard Schlenk techniques and a Vacuum Atmospheres HE-493 drybox unless otherwise mentioned. All solvents were dried and purified prior to use following standard techniques. The metal salts were purchased from Sigma-Aldrich or Strem Chemicals and were used as received. The complexes $[Cu_2(\mu\text{-F})(\mu\text{-}\mathbf{L}_m)_2](BF_4)_3$, $[Cu_2(\mu\text{-F})(\mu\text{-}\mathbf{L}_m\text{*})_2](ClO_4)_3$, and $[Cu_2(\mu\text{-Cl})(\mu\text{-}\mathbf{L}_m\text{*})_2](ClO_4)_3$ were prepared according to reported procedures.[2,8]

Crystals used for elemental analysis and mass spectrometry were removed from the mother liquor, rinsed with ether, and dried under a vacuum. Elemental analyses were performed on samples dried to constant weight, which removed the solvent of crystallization, by Robertson Microlit Laboratories (Ledgewood, NJ). Mass spectrometric measurements were obtained on a MicroMass QTOF spectrometer in an acid-free environment. For all reported peaks, the isotopic patterns match those calculated for the assignments.

Caution: Although no problems were encountered with perchlorate salts and $(CH_3)_3SiN_3$ during this work, these compounds should be considered potentially explosive!

High-field, high-frequency EPR spectra at temperatures ranging from ca. 6 K to 290 K were recorded on a home-built spectrometer at the EMR facility of the NHMFL.[9] The instrument is a transmission-type device in which microwaves are propagated in cylindrical lightpipes. The microwaves were generated by a phase-locked Virginia Diodes source generating frequency of 13 ± 1 GHz and producing its harmonics of which the second, fourth, sixth, eighth, 16th, 24th, and 32nd were available. A superconducting magnet (Oxford Instruments) capable of reaching a field of 17 T was employed. The powder samples were not constrained and showed no magnetic torqueing at high magnetic fields. Additionally, X-band and Q-Band spectra were recorded on a Bruker ElexSys E500 instrument equipped with an NMR teslameter ER 036TM and a frequency counter E 41 FC (Faculty of Chemistry, Wroclaw University).

Magnetic susceptibility measurements over the temperature range 1.8−300 K were performed at a magnetic field of 0.5 T using a Quantum Design SQUID MPMSXL-5 magnetometer. Correction for the sample holder, as well as the diamagnetic correction χ_D, which was estimated from the Pascal constants,[10] was applied.

$[Cu_2(\mu\text{-CN})(\mu\text{-}\mathbf{L}_m)_2](ClO_4)_3$, ***1***. A mixture of $Cu(ClO_4)_2\cdot 6H_2O$ (0.186 g, 0.50 mmol) and NaCN (0.016 g, 0.25 mmol) were dissolved in MeOH (6 mL). The ligand, $\mathbf{L}_m$ (0.186 g, 0.50 mmol), dissolved in MeOH (8 mL), was transferred by cannula into the copper(II) solution. A deep blue precipitate formed immediately. The reaction mixture was stirred for 6 h, after which time the system was filtered by cannula, and the remaining solid was washed with 5 mL of ether and dried in a vacuum overnight, affording 0.273 g (75%) of the crude product. Single crystals suitable for X-ray and other studies were grown by vapor diffusion of Et_2O into concentrated 1 mL acetonitrile solutions of **1** and were isolated as **1**·3CH_3CN. Anal. Calcd (Found) for $C_{41}H_{36}Cl_3Cu_2N_{17}O_{12}$: C, 41.30 (41.08); H, 3.04 (2.87); N, 19.97 (19.67). MS ESI(+) *m*/*z* (rel. % abund.) [assgn]: 1092 (2) $[Cu_2(\mathbf{L}_m)_2(CN)(ClO_4)_2]^+$, 497 (10) $[Cu_2(\mathbf{L}_m)_2(CN)(ClO_4)]^{2+}$, 433 (100) $[Cu(\mathbf{L}_m)]^+$, 371 (18) $[\mathbf{L}_m + H]^+$, 298 (60) $[Cu_2(\mathbf{L}_m)_2(CN)]^{3+}$.

$[Cu_2(\mu\text{-}N_3)(\mu\text{-}\mathbf{L}_m)_2](BF_4)_3$, ***2***. In the drybox, $[Cu_2(\mu\text{-F})(\mu\text{-}\mathbf{L}_m)_2](BF_4)_3$ (0.150 g, 0.131 mmol) was dissolved in CH_3CN (5 mL). Upon addition of 0.02 mL (0.018 g, 0.15 mmol) of $(CH_3)_3SiN_3$, the blue solution turned green. Vapor diffusion of Et_2O into the green solution, further diluted with a small amount of CH_3CN, resulted in crystals of **2**·2.25CH_3CN (0.080 g, 52%). Anal. Calcd (Found) for $C_{40}H_{36}B_3Cu_2N_{19}F_{12}$: C, 41.05 (41.22); H, 3.10 (2.85); N, 22.74 (22.51). MS ESI(+) *m*/*z* (rel. % abund.) [assgn]: 1082 (2) $[Cu_2(\mathbf{L}_m)_2(N_3)(BF_4)_2]^+$, 498 (2) $[Cu_2(\mathbf{L}_m)_2(N_3)(BF_4)]^{2+}$, 433 (100) $[Cu(\mathbf{L}_m)]^+$, 371 (40) $[\mathbf{L}_m + H]^+$, 303 (50) $[Cu_2(\mathbf{L}_m)_2(N_3)]^{3+}$.

$[Cu_2(\mu\text{-CN})(\mu\text{-}\mathbf{L}_m\text{*})_2](ClO_4)_3$, ***3***. Compound **3** was synthesized similarly to compound **1** starting from $Cu(ClO_4)_2\cdot 6H_2O$ (0.190 g, 0.514 mmol), NaCN (0.017 g, 0.26 mmol), and $\mathbf{L}_m$* (0.248 g, 0.514 mmol). The solution went through a series of color changes followed by the formation of a blueish-green precipitate, 0.273 g (75%). Single crystals were grown by vapor diffusion of Et_2O into concentrated 1 mL acetonitrile solutions of **3** and were isolated as **3**·2CH_3CN. Anal. Calcd (Found) for $C_{57}H_{68}Cl_3Cu_2N_{17}O_{12}$: C, 48.32 (47.97); H, 4.84 (4.58); N, 16.81 (16.59). MS ESI(+) *m*/*z* (rel. % abund.) [assgn]: 1316 (8) $[Cu_2(\mathbf{L}_m\text{*})_2(CN)(ClO_4)_2]^+$, 609 (20) $[Cu_2(\mathbf{L}_m\text{*})_2(CN)(ClO_4)]^{2+}$, 545 (100) $[Cu(\mathbf{L}_m\text{*})]^+$, 483 (55) $[\mathbf{L}_m\text{*} + H]^+$, 373 (95) $[Cu_2(\mathbf{L}_m\text{*})_2(CN)]^{3+}$.

$[Cu_2(\mu\text{-}\mathbf{L}_m\text{*})(\mu\text{-}N_3)_2(N_3)_2]$, ***4***. The complex $[Cu_2(\mu\text{-Cl})(\mu\text{-}\mathbf{L}_m\text{*})_2](ClO_4)_3$ (0.020 g, 0.014 mmol) was dissolved in CH_3CN (2 mL). To this solution, NaN_3 (0.005 g, 0.08 mmol) dissolved in CH_3CN (1 mL) and MeOH (1 mL) was added dropwise. The solution immediately turned dark green. Single crystals suitable for X-ray and the other studies were grown by vapor diffusion of Et_2O into this dark green solution and resulted in crystals of **4** (0.009 g, 83%). Anal. Calcd (Found) for $C_{28}H_{34}Cu_2N_{20}$: C, 43.24 (42.88); H, 4.41 (4.06); N, 36.02 (36.51).

$[Cu_5(\mu\text{-}I_4)(\mu\text{-}\mathbf{L}_m\text{*})_2](I_3)$, ***5***. In the drybox, $[Cu_2(\mu\text{-F})(\mu\text{-}\mathbf{L}_m\text{*})_2](ClO_4)_3$ (0.150 g, 0.106 mmol) was dissolved in 5 mL of CH_3CN. Upon addition of three drops of $(CH_3)_3SiI$, the green solution turned brown. Vapor diffusion of Et_2O into the brown solution resulted in single crystals of **5** (0.030 g, 39%). Anal. Calcd (Found) for $C_{56}H_{68}Cu_5N_{16}I_7$: C, 30.98 (31.41); H, 3.16 (2.78); N, 10.32 (10.21). MS ESI(+) *m*/*z* (rel. % abund.) [assgn]: 1027 (2) $[Cu(\mathbf{L}_m\text{*})_2]^+$, 737 (100) $[Cu_4(\mathbf{L}_m\text{*})_2(I_2)]^{2+}$, 545 (92) $[Cu(\mathbf{L}_m\text{*})]^+$, 483 (20) $[\mathbf{L}_m\text{*} + H]^+$.

Crystallographic Studies. X-ray diffraction intensity data for compounds **1**−**5** were measured on a Bruker SMART APEX CCD-based diffractometer (Mo Kα radiation, λ = 0.71073 Å).[11] The raw area detector data frame processing was performed with the SAINT+ and SADABS programs.[12] Final unit cell parameters were determined by least-squares refinement of large sets of strong reflections taken from each data set. Direct methods structure solution, difference Fourier calculations, and full-matrix least-squares refinement against F^2 were performed with SHELXS/L[2] as implemented in OLEX2.[13] Non-hydrogen atoms were refined with anisotropic displacement

DOI: 10.1021/ic502485p
Inorg. Chem. 2015, 54, 1487−1500

Table 1. Selected Crystal Data and Structure Refinement

	1·3CH_3CN	2·2.25CH_3CN	3·2CH_3CN	4	5
formula	$C_{47}H_{45}Cl_3Cu_2N_{20}O_{12}$	$C_{44.50}H_{42.75}B_3Cu_2F_{12}N_{21.25}$	$C_{61}H_{74}Cl_3Cu_2N_{19}O_{12}$	$C_{28}H_{34}Cu_2N_{20}$	$C_{56}H_{68}Cu_5I_7N_{16}$
fw, g mol^{-1}	1315.46	1262.79	1498.82	777.83	2171.66
cryst syst	triclinic	monoclinic	monoclinic	monoclinic	monoclinic
space group	$P\bar{1}$	$P2_1$	$C2/c$	$C2/c$	$C2/m$
T, K	100(2)	100(2)	100(2)	100(2)	100(2)
a, Å	10.0369(18)	12.8682(18)	23.910(7)	23.0409(12)	19.632(2)
b, Å	13.096(2)	13.9995(19)	12.374(4)	8.7757(5)	21.904(3)
c, Å	22.234(4)	15.841(2)	23.705(7)	19.4868(10)	8.5445(10)
α, deg	94.415(4)	90	90	90	90
β, deg	93.120(5)	111.853(3)	103.733(6)	118.2850(10)	96.768(2)
γ, deg	109.393(4)	90	90	90	90
V, $Å^3$	2738.5(9)	2648.7(6)	6813(4)	3469.8(3)	3648.8(7)
Z	2	2	4	4	2
R_1 ($I > 2\sigma(I)$)	0.0497	0.0550	0.0376	0.0366	0.0427
wR_2 ($I > 2\sigma(I)$)	0.0773	0.1326	0.0944	0.0901	0.1065

parameters, the exception being disordered species. The hydrogen atoms were placed in geometrically idealized positions and included as riding atoms. Details of the data collection are given in Table 1.

For compound 1·3CH_3CN the asymmetric unit consists of half of two independent $[Cu_2(\mu\text{-}CN)(\mu\text{-}\mathbf{L}_m)_2]^{3+}$ cations, three independent perchlorate anions, and three independent acetonitrile molecules. The two independent cations are located on crystallographic inversion centers, imposing disorder on the bridging CN^- groups. For refinement, a single atomic position with a 50/50 population of carbon and nitrogen was used for each cation. With this model, the C2/N2 anisotropic displacement parameters are slightly elongated, suggesting a disorder somewhat beyond a single scrambled C/N position. However, this disorder was too small to be modeled well crystallographically. One perchlorate anion (Cl3) is disordered and was modeled with two components. The major disorder fraction is Cl3A = 0.909(6). The geometry of the minor component was restrained to be similar to the major (SHELX SADI instruction). The largest residual electron density peak of 0.59 $e^-/Å^3$ in the final difference map is located 0.08 Å from Cu2.

For compound 2·2.25CH_3CN the space groups $P2_1$ and $P2_1/m$ were consistent with the pattern of systematic absences in the intensity data. $P2_1$ was established as the correct space group by the structure solution. The ADDSYM program in PLATON found no missed symmetry elements.[14] The asymmetric unit consists of one $[Cu_2(\mu\text{-}N_3)(\mu\text{-}\mathbf{L}_m)_2]^{3+}$ cation, three tetrafluoroborate anions, and a region of disordered acetonitrile solvent molecules. Each BF_4^- anion is disordered over two closely separated positions with occupancies B1A/B1B = 0.79(1)/0.21(1), B2A/B2B = 0.65(1)/0.35(1), B3A/B3B = 0.71(1)/0.29(1). Total site occupancy was constrained to sum to unity. B−F and F−F distance restraints were applied to maintain chemically reasonable geometries for each component. The acetonitrile disorder was modeled with four molecules of variable occupancy: N1S = 0.88(1), N2S = N4S = 0.5, and N3S = 0.38(1). Occupancies of acetonitrile molecules N2S and N4S were fixed to avoid physically nonsensical values, and C−N and C−C distance restraints were applied. The largest residual electron density peak of 0.62 $e^-/Å^3$ in the final difference map is located 1.0 Å from Cu1. The final absolute structure (Flack) parameter refined to 0.004(14).

For compound 3·2CH_3CN the asymmetric unit consists of half of one $[Cu_2(\mu\text{-}CN)(\mu\text{-}\mathbf{L}_m{*})_2]^{3+}$ cation located on an inversion center, 1.5 perchlorate anions and one acetonitrile molecule. The bridging cyano group is disordered and was modeled with one atomic position consisting of 50% carbon and 50% nitrogen. Perchlorate anion Cl2/O21−O24 is disordered about a C_2 axis of rotation, and therefore only half of this anion is present per asymmetric unit. This perchlorate is further disordered over two independent positions within the asymmetric unit. The occupancies of the disordered groups are A/B = 0.057(2)/0.443(2), which were constrained to sum to 0.5. Geometries of the two independent disordered groups were restrained to be similar to that of the ordered perchlorate Cl1/O11−O14 with SHELX SAME instructions (30 restraints).

The asymmetric unit of compound 4 consists of one copper atom, half of one ligand, which is located on a 2-fold axis of rotation, and two azide ions. The 2-fold axis passes through phenyl ring atoms C4 and C5 of the $\mathbf{L}_m{*}$ ligand.

For 5 there is disorder of both the cation and the two independent anion sites in the crystal; trial solutions in the space groups $C2$ and Cm also resulted in the same disorder discussed below. The asymmetric unit in $C2/m$ consists of 1/4 of one $[Cu_5(\mu\text{-}I_4)(\mu\text{-}\mathbf{L}_m{*})_2]^+$ cation, which has crystallographic C_{2h} point symmetry, and two regions of triiodide anions. The cation consists of two independent copper(I) sites, two bridging iodide atoms, and half of one $\mathbf{L}_m{*}$ ligand. Atoms I1, C4, and C5 sit on a mirror plane; atoms Cu2 and I2 reside on the C_2 axis perpendicular to the mirror. Atom Cu2 is disordered across the nearby mirror plane and was refined with half-occupancy. Refining Cu2 with full occupancy results in a very short Cu2−Cu2′ distance of ca. 2.1 Å and an unacceptably large displacement parameter. Triiodide anion I_3/I_4 consists of two independent iodine atoms and also has C_{2h} point symmetry. I_3 is located on the C_{2h} site, and I_4 is disordered about the C_2 axis over two positions. The displacement parameters of atoms I_3 and I_4 became unreasonably large when refined with full occupancy. Allowing their site occupancies to refine decreased the R_1 value by ca. 2% and gave acceptable displacement parameters. The final population of the I_3/I_4 anion is 84%. The deficit of negative charge caused by the partial occupancy of I_3/I_4 is compensated by the second independent anion region, which is severely disordered about a crystallographic site with C_{2h} point symmetry. No chemically recognizable species could be found. Instead, an essentially continuous linear distribution of electron density extending along the y-axis from $y = 0.3$ to $y = 0.7$ was observed. This was interpreted as disordered I_3^- species. For refinement, six electron density peaks found in this region were assigned as iodine atoms I5−I10, and their occupancy values were allowed to vary freely. These atoms were all assigned a fixed displacement parameter of 0.07 $Å^2$, which was chosen because it gave a final composition of three iodine atoms per $[Cu_5(\mu\text{-}I_4)(\mu\text{-}\mathbf{L}_m{*})_2]^+$ unit, i.e., an electroneutral crystal. The chemical occupancies of the individual iodine atom peaks are low, ca. 3%. It is likely that when these atoms are not present in a given asymmetric unit, a linear guest molecule such as the crystallization solvent acetonitrile is present, but this could not be identified because of the disorder.

RESULTS

Synthesis. The reactions of $Cu(ClO_4)_2$ with NaCN and the ligands $\mathbf{L}_m$ or $\mathbf{L}_m{*}$ result in the cyanide bridged metallacycles 1 and 3, respectively. Compound 2 was synthesized starting from the previously reported F^- bridged metallacycle of the ligand $\mathbf{L}_m$.[8] The bridging F^- is exchanged with N_3^- in the presence of

DOI: 10.1021/ic502485p
Inorg. Chem. 2015, 54, 1487−1500

$(CH_3)_3SiN_3$. The driving force of this reaction is the formation of strong Si−F bonds. The reactions are shown in Scheme 2.

Scheme 2. Synthesis of Compounds 1−5

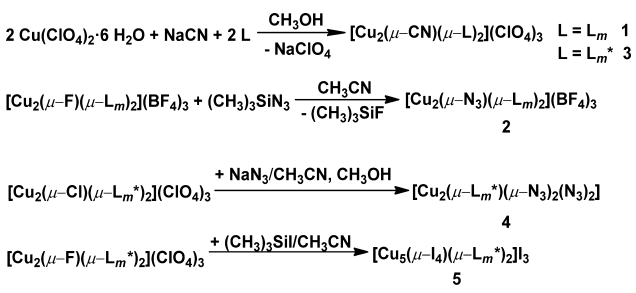

These metallacycles are stable in solution as MS ESI(+) spectra show peaks with proper isotopic distributions for all three $[Cu_2(\mathbf{L})_2(\mu\text{-X})(\text{counterion})_x]^{(3-x)+}$ cations. An alternate synthesis of **2** from the reaction of the building blocks of the metallacycle: $Cu(ClO_4)_2{\cdot}6H_2O$, NaN_3 and $\mathbf{L}_m$ results in both the azide bridged compound, $[Cu_2(\mu\text{-}N_3)(\mu\text{-}\mathbf{L}_m)_2](ClO_4)_3$ and the analogous hydroxide bridged compound.[2b]

We isolated the polymeric structure $[Cu_2(\mu\text{-}\mathbf{L}_m{}^*)(\mu\text{-}N_3)_2(N_3)_2]$ (**4**) upon the reaction of $[Cu_2(\mu\text{-Cl})(\mu\text{-}\mathbf{L}_m{}^*)_2](ClO_4)_3$ with a large excess of NaN_3; a reaction using stoichiometric amounts of azide did not yield the desired $[Cu_2(\mu\text{-}N_3)(\mu\text{-}\mathbf{L}_m{}^*)_2](ClO_4)_3$ complex. Attempts to synthesize the I^- bridged dinuclear copper(II) metallacycle failed, and instead we isolated a pentametallic species, $[Cu_5(\mu\text{-}I_4)(\mu\text{-}\mathbf{L}_m{}^*)_2]I_3$ (**5**), upon the reaction of the fluoride bridged metallacycle with $(CH_3)_3SiI$. The copper(II) centers of the starting material were reduced to copper(I) during this reaction.

Solid State Structures. Figure 1 shows the two independent cationic units in the crystal structure of $[Cu_2(\mu\text{-CN})(\mu\text{-}\mathbf{L}_m)_2](ClO_4)_3{\cdot}3CH_3CN$, **1**·3$CH_3CN$. Similarly, Figure 2 shows the structure for the cationic units of $[Cu_2(\mu\text{-}N_3)(\mu\text{-}\mathbf{L}_m)_2](BF_4)_3{\cdot}2.25CH_3CN$, **2**·2.25$CH_3CN$ and $[Cu_2(\mu\text{-CN})(\mu\text{-}\mathbf{L}_m{}^*)_2](ClO_4)_3{\cdot}2CH_3CN$, **3**·2$CH_3CN$, respectively. Selected structural parameters are shown in Table 2.

The single end-to-end bridging cyano groups of **1**·3CH_3CN and **3**·2CH_3CN are disordered about the inversion center, effectively scrambling the carbon and nitrogen atoms. This group was modeled with one atomic position consisting of 50% carbon and 50% nitrogen; in Figures 1 and 2b both are labeled N1 (N2). The Cu−N(C)−N(C)−Cu′ torsion angle is 180.0° in both compounds. The two atoms labeled N1 are slightly displaced with respect to the Cu−Cu axis, one being slightly in front, and the other being at the back of the Cu···Cu axis, the Cu−N(C)−N(C) angles are 176.9° and 173.9° for **1**·3CH_3CN and 173.0° for **3**·2CH_3CN. The geometry around copper(II) in these complexes is distorted trigonal bipyramidal. Using the τ_5 values a measure of the geometry in five coordinate systems,[15] where a perfect square pyramid has a τ_5 value of 0 and a perfect trigonal bipyramid has a value of 1, **1**·3CH_3CN (τ_5 = 0.76/0.79) is closer to being trigonal bipyramidal than **3**·2CH_3CN (τ_5 = 0.61).

For **1**·3CH_3CN, the axial positions are occupied by N21, N41 (N21−Cu1−N41 177.70°) for one of the two independent cations in the unit cell and N61, N81 (N61−Cu2−N81 177.29°) for the second cation. The atoms N1, N11, N31, and N2, N51, N71 reside in the equatorial plane, with angles in the range of 104.18−132.00°. The pyrazolyl Cu−N bond lengths show a slightly compressed trigonal bipyramidal geometry, axial Cu−N bonds are between 1.98 and 2.01 Å, and equatorial Cu−N bond lengths are between 2.06 and 2.09 Å.

For **3**·2CH_3CN the axial positions are occupied by N21, N41 (N21−Cu1−N41 173.56°), while N1, N11, N31 reside in the equatorial plane, these angles being 103.59°, 119.29°, and 137.11° approximating a trigonal bipyramid. Conversely, by analyzing the Cu−N bond lengths the geometry resembles more a distorted square pyramidal geometry, with axial N31 (Cu1−N31 2.1297 Å) and equatorial N1, N11, N21, and N41, these latter four bond lengths being 0.1 Å shorter than Cu1−N31 (Table 2), as expected for pseudo Jahn−Teller distorted square pyramidal geometries.[16]

The single bridging azide in **2**·2.25CH_3CN adopts end-on coordination mode, by bridging the two copper(II), Cu1−N1−Cu2 angle being 138.0° and the Cu1···Cu2 nonbonding distance is 3.084 Å. The nitrogen donor atoms around the metal centers are in pseudo Jahn−Teller distorted square pyramidal geometry (τ_5 = 0.30/0.26), with axial Cu1−N51 2.195 Å, and Cu2−N71 2.176 Å. The equatorial Cu−N bond lengths vary between 1.988 and 2.059 Å, the longest being those involving the azide, N1.

Although very different, in the structure of $[Cu_2(\mu\text{-}\mathbf{L}_m{}^*)(\mu\text{-}N_3)_2(N_3)_2]$ (**4**) the copper(II) centers are still five coordinate, by coordination of two ligand nitrogens and three azide nitrogens (Figure 3 and Table 2). The geometry is square pyramidal, τ_5 = 0.11. The azide N31−N32−N33 is end-to-end coordinated and N33 becomes the axial ligand, Cu1−N33 being 2.383 Å. The equatorial positions are occupied by N11, N21, N31, and N41, and the average of these bonds is 2.00 Å.

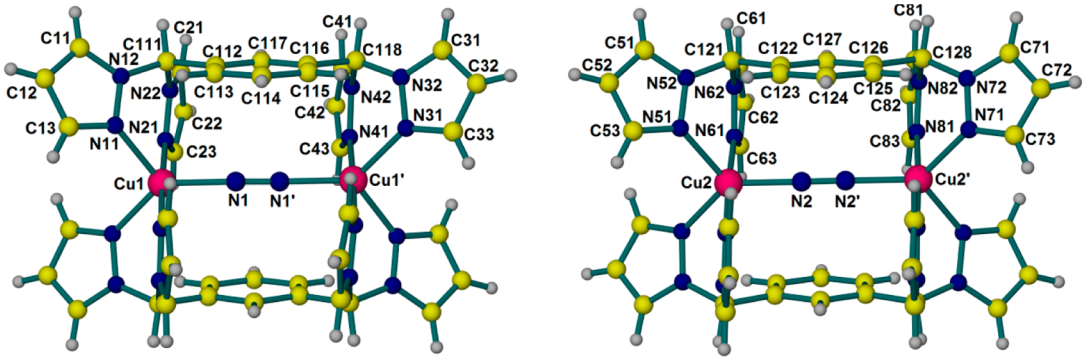

Figure 1. Structure of the two independent cationic units of $[Cu_2(\mu\text{-CN})(\mu\text{-}\mathbf{L}_m)_2](ClO_4)_3{\cdot}3CH_3CN$ (**1**·3CH_3CN). The atoms in the disordered CN^- bridge were modeled as 50% carbon and 50% nitrogen, but both are labeled N1 (N2).

DOI: 10.1021/ic502485p
Inorg. Chem. 2015, 54, 1487−1500

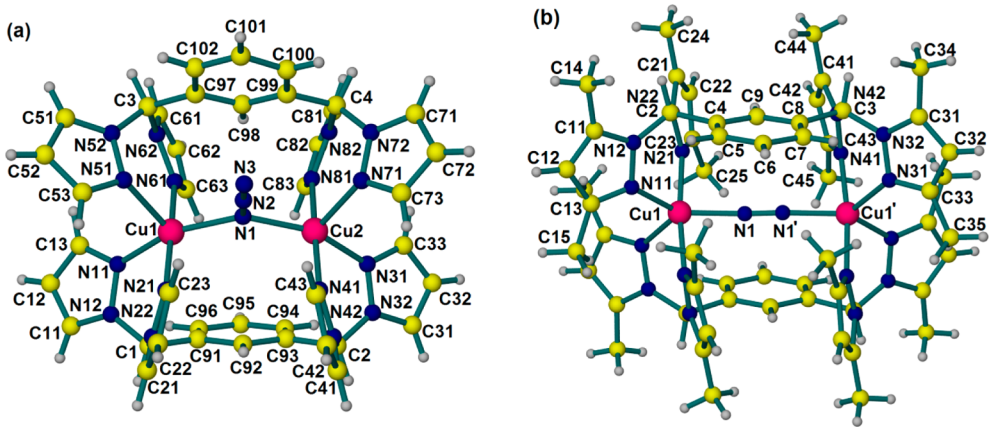

Figure 2. Structure of the cationic unit of (a) $[Cu_2(\mu\text{-}N_3)(\mu\text{-}L_m)_2](BF_4)_3{\cdot}2.25CH_3CN$ (**2**·2.25CH_3CN) (b) $[Cu_2(\mu\text{-}CN)(\mu\text{-}L_m{*})_2](ClO_4)_3{\cdot}2CH_3CN$ (**3**·2CH_3CN), where the atoms in the disordered CN^- bridge were modeled as 50% carbon and 50% nitrogen, but both are labeled N1.

Table 2. Important Structural Parameters for $[Cu_2(\mu\text{-}CN)(\mu\text{-}L_m)_2](ClO_4)_3{\cdot}3CH_3CN$ (1**·3CH_3CN), $[Cu_2(\mu\text{-}N_3)(\mu\text{-}L_m)_2](BF_4)_3{\cdot}2.25CH_3CN$ (**2**·2.25CH_3CN), $[Cu_2(\mu\text{-}CN)(\mu\text{-}L_m{*})_2](ClO_4)_3{\cdot}2CH_3CN$ (**3**·2CH_3CN) and $[Cu_2(\mu\text{-}L_m{*})(\mu\text{-}N_3)_2(N_3)_2]$ (**4**)**

	1·3CH_3CN	**2**·2.25CH_3CN	**3**·2CH_3CN	**4**
temp, K	100(2)	100(2)	100(2)	100(2)
metal centers	Cu(1,2)−Cu(1,2)	Cu(1)−Cu(2)	Cu(1)−Cu(1)′	Cu(1)−Cu(1)′
bridging Cu−N−Cu or Cu−N(C)−N(C), deg	177.0(6)/174.0(7)	138.0(2)	173.0(3)	113.3 (2)/122.2(2)
Cu−N1(2) or Cu−N33, Å	1.946(4)/1.926(4)	2.054(4)/ 2.059(4)	1.948(2)	2.3825(19)
Cu−N11/Cu−N51, Å	2.092(4)/2.090(4)	2.017(5)/ 2.195(5)	2.0368(17)	2.0393(17)
Cu−N21/Cu−N61, Å	1.997(4)/1.995(4)	2.005(4)/ 1.988(5)	2.0355(16)	2.0169(18)
Cu−N31/Cu−N71, Å	2.055(4)/2.056(4)	2.036(5)/ 2.176(5)	2.1297(17)	1.9799(18)
Cu−N41/Cu−N81, Å	1.981(4)/2.006(4)	2.004(5)/ 2.007(5)	2.0365(17)	1.974(2)
τ_5	0.76/0.79	0.30/0.26	0.61	0.11
Cu···Cu, Å	5.049/5.009	3.084	5.024	4.881

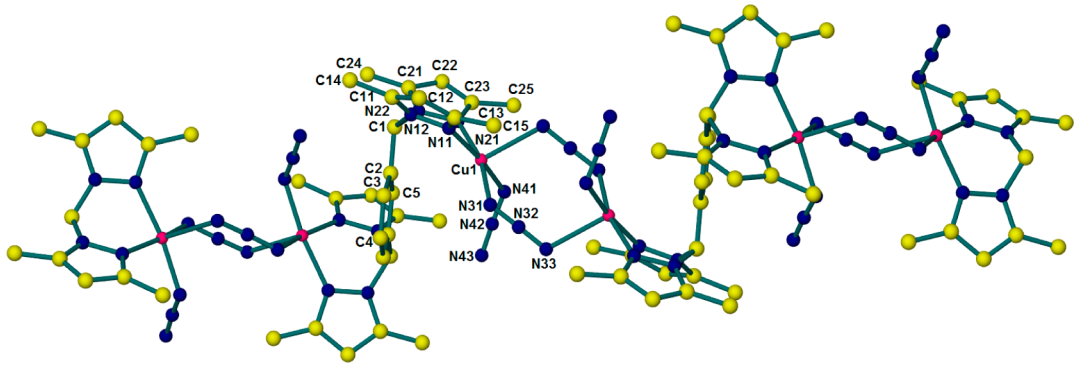

Figure 3. Polymeric structure of $[Cu_2(\mu\text{-}L_m{*})(\mu\text{-}N_3)_2(N_3)_2]$ (**4**). Hydrogen atoms are omitted for clarity.

The Cu−N bonds involving the ligand are slightly shorter than the azide Cu−N bonds by approximately 0.04 Å. The ligand L_m* adopts the *anti*-conformation, with two bis(pyrazolyl)-methane units being on the opposite side of the phenylene spacer. The infinite parallel polymeric chains, formed by L_m* and two end-to-end azides alternately bridging two copper(II) centers, run along the crystallographic [101] direction.

Figure 4 presents the structure of the cationic unit of $[Cu_5(\mu\text{-}I_4)(\mu\text{-}L_m{*})_2]I_3$ (**5**) and Table 3 contains selected structural parameters for this compound. The asymmetric unit contains 1/4 of one cation, and therefore all four Cu1 centers are identical. These four copper(I) centers are in a distorted tetrahedral coordination environment where the N11−Cu1−N21 angle is 93.78°, the I1−Cu1−I2 angle is 110.76,° and the N−Cu1−I angles vary between 110.02° and 116.31°. Two pairs of Cu1 centers are bridged by the ligand L_m* and I1, with Cu1−I1−Cu1 bridging angle 120.34°. The two pairs of Cu1 centers are connected via I2 bridges with a Cu1−I2−Cu1 angle of 116.21°. The Cu2 cation resides in the cavity formed by the four Cu1 ions alternating with two I1 and two I2 ions. The Cu2 cation is disordered across a mirror plane and is refined with half-occupancy. The geometry around Cu2 is more unusual, trigonal planar, Cu2 being exactly in the least-squares mean plane defined by the four Cu1 and I1 atoms, with Cu1−I1−Cu2 59.35°, Cu1−I2−Cu2 58.11°, I1−Cu2−I1 131.11°, and I1−Cu2−I2 114.45°.

Magnetic Susceptibility. The magnetic data for compounds **1**−**3** are shown in Figure 5. The complexes exhibit strong antiferromagnetic coupling, although it is much smaller than in the halide- and hydroxide-bridged copper complexes of

DOI: 10.1021/ic502485p
Inorg. Chem. 2015, 54, 1487−1500

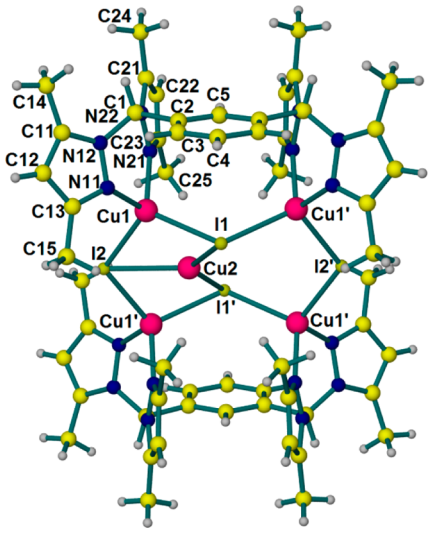

Figure 4. Structure of the cationic unit of $[Cu_5(\mu\text{-}I_4)(\mu\text{-}L_m{*})_2]I_3$ (**5**); Cu2 is disordered across the mirror plane and is refined with half-occupancy (only one of the two Cu2 sites is shown).

Table 3. Selected Structural Parameters for $[Cu_5(\mu\text{-}I_4)(\mu\text{-}L_m{*})_2]I_3$ (5)

temp, K	100(2)
Cu1−I1−Cu1	120.34(3)
Cu1−I2−Cu1	116.21(3)
Cu1−I1−Cu2	59.35(3)
Cu1−I2−Cu2	58.10(2)
I1−Cu1−I2	110.76(3)
I1−Cu1−N11	110.76(14)
I1−Cu1−N21	116.31(13)
I2−Cu1−N11	110.02(14)
I2−Cu1−N21	113.95(14)
N11−Cu1−N21	93.78(18)
I1−Cu2−I1	131.11(7)
I1−Cu2−I2	114.45(4)
Cu1−I1, Å	2.6411(7)
Cu1−I2, Å	2.6305(8)
Cu2−I1, Å	2.5219(9)
Cu2−I2, Å	2.6374(19)
Cu−N11, Å	2.047(5)
Cu−N21, Å	2.041(4)
Cu1···Cu1′, Å	2.5581(11)
Cu1···Cu2, Å	2.5581(11)

the same ligands. Monomeric contamination is seen in each case and is much smaller for **3** (0.2%) than for **2** or **1** (2.4% and 1.4%, respectively). The magnetic susceptibility data were interpreted using the standard Heisenberg−Dirac−Van Vleck Hamiltonian: $\hat{\mathbf{H}} = -J\hat{\mathbf{S}}_1\hat{\mathbf{S}}_2$. In this notation, J is negative in the case of antiferromagnetic superexchange interactions. The magnetic susceptibility of a dinuclear copper(II) system is

$$\chi_d = \frac{N\mu_B^2 g^2}{3kT}\frac{6\exp(J/kT)}{1+3\exp(J/kT)} + 2TIP \quad (1)$$

The monomer susceptibility can be calculated from

$$\chi_m = (N\mu^2B^2g^2/3kT)0.75 + TIP \quad (2)$$

and the total susceptibility can be expressed as

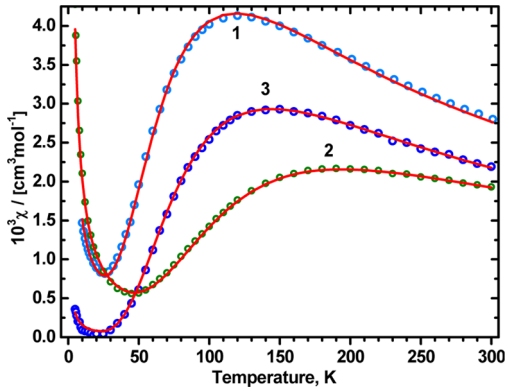

Figure 5. Circles: Experimental magnetic susceptibility per mole of $[Cu_2(\mu\text{-}CN)(\mu\text{-}L_m)_2](ClO_4)_3$ (**1**), $Cu_2(\mu\text{-}N_3)(\mu\text{-}L_m)_2](BF_4)_3$ (**2**), and $[Cu_2(\mu\text{-}CN)(\mu\text{-}L_m{*})_2](ClO_4)_3$ (**3**). Lines: calculated with g_{ave} = 2.24, $-J$ = 135 cm^{-1}, f = 0.014 (f = fraction of monomeric impurities) for **1**, g_{ave} = 2.07, $-J$ = 223 cm^{-1}, f = 0.024 for **2** and g_{ave} = 2.12, $-J$ = 161 cm^{-1}, f = 0.002 for **3**.

$$\chi = (1-f)\chi_d + 2f\chi_m \quad (3)$$

where f is the fraction of monomeric impurities. The magnetic susceptibility data (Figure 5) were fitted to 3 using a nonlinear least-squares routine. The calculated exchange parameters J are listed in Table 4.

EPR Spectra. Well resolved high-field (Figures 6−8 and S1) as well as X and Q-Band EPR spectra (Figures S3 and S4) were observed for the CN^- bridged compounds **1** and **3**, over a wide temperature range between ca. 20 K and room temperature. Hyperfine structure due to two copper nuclei was observed in the powder X-Band spectra of **3** at 80 K (Figure S4), only on the "half-field" transition. Frozen solution spectra (only **3** was sufficiently soluble), unfortunately, do not exhibit better resolution. They look very similar to the powder spectra and prove that the complex does not dissociate into monomers in a CH_3CN solution (Figure S1B). No usable spectra could be obtained for the azido-bridged copper(II) complex. The spectra were interpreted by using the standard spin Hamiltonian for S = 1

$$\hat{\mathbf{H}} = \mu_B\mathbf{B}\cdot\{\mathbf{g}\}\cdot\hat{\mathbf{S}} + D\{\hat{\mathbf{S}}_z^2 - S(S+1)/3\} + E(\hat{\mathbf{S}}_x^2 - \hat{\mathbf{S}}_y^2) \quad (4)$$

The simulation of the spectra of **3** was successful, particularly at room temperature (Figure S1). Problems in the intensity pattern in the simulations of **1** (Figure 6) are likely caused by the presence of two slightly different molecules, as revealed by the X-ray structure. The spectra of two species do not differ sufficiently to be resolved. Like in the other copper(II) complexes of $\mathbf{L}_m$ and $\mathbf{L}_m{*}$, the g_x, g_y, and g_z values in **1** and **3** are very different from each other, with the g_x value approximately equal to the average of g_y and g_z, and one of them is very close to 2 indicating the d_{z^2} ground state of the copper(II) ions.[2] These results are supported by the DFT calculations (see details below). DFT typically underestimates the g values for copper(II) complexes, but offers insight into the g component orientations.[17] Thus, the smallest g component lies according to DFT just 4.5° from the vertical axis of the trigonal bipyramid (defined as the vector perpendicular to the plane of three equatorial ligands, either NNN or NNC), both on the C-side and the N-side of the CN bridge. The direction of the intermediate g component is 5° apart from the Cu−

DOI: 10.1021/ic502485p
Inorg. Chem. 2015, 54, 1487−1500

Table 4. Magnetic Properties, Results of the "Broken Symmetry" DFT Calculations and the Spin Hamiltonian Parameters

complex	**1**[a]	**3**	**2**[b]	$[Cu_2(\mu\text{-}Cl)(\mathbf{L}_m\text{*})_2](ClO_4)_3$	$[Cu_2(\mu\text{-}OH)(\mathbf{L}_m)_2](ClO_4)_3\cdot 2H_2O$[b]
τ_5	0.79	0.61	0.30	0.70	0.30
			Spin Population		
Cu	0.65 (N side)	0.65 (N side)	0.614	0.635	0.658
	0.60 (C side)	0.61 (C side)			
bridge	0.090 (N)	0.092 (N)	0.138 (C)	0.058 (Cl)	0.153 (O)
	0.136 (C)	0.13 (N)			
N on trigonal axis	0.105	0.106	0.094	0.100	0.094
	0.114	0.113	0.092	0.101	0.085
N in trigonal plane	0.041	0.043	0.080	0.048	0.074
	0.028	0.012	0.006	0.038	0.005
overlap integral	0.071	0.069	0.166	0.189	0.172
$E_{antisym} - E_{sym}$ (cm^{-1})	3630	3980	5340	5940	5710
			Exchange Integral $-J$, cm^{-1}		
calc, DFT	160 (151)[c]	152	403	914	700
exp	130	161	223	720	555
			Spin Hamiltonian Parameters (150 K)		
g_x	2.129	2.125		2.185	2.130[d]
g_y	2.242	2.248		2.246	2.263[d]
g_z	2.009	2.018		2.000	2.048[d]
D, cm^{-1}	0.0476	0.0327		0.182	0.199[d]
E, cm^{-1}	0.0373	0.0308		0.046	0.136[d]

[a]Results shown are for the molecule with short Cu···Cu distance (5.01 Å). [b]The trigonal bipyramidal description is used for easy comparison to other compounds in Table 4. [c]J calculated for the molecule with Cu···Cu = 5.04 Å given in parentheses. [d]When choosing the direction of the largest g component as "Z", an equivalent parameter set is obtained: g_x = 2.130, g_y = 2.048 g_z = 2.263, D = 0.299 cm^{-1}, E = 0.028 cm^{-1}.[2b]

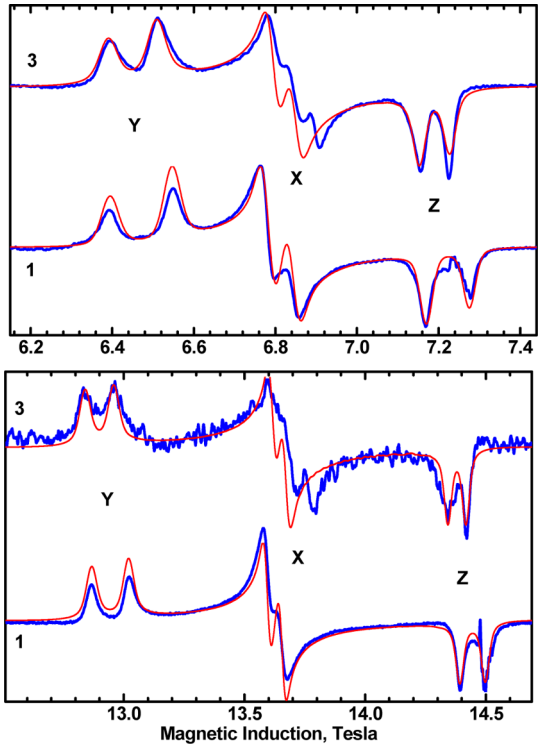

Figure 6. EPR spectra of **1** and **3** recorded at 150 K with ν = 203.2 GHz (top) and with 406.4 GHz (bottom). Blue: experimental; red: simulated with parameters from Table 4. The feature seen in the 203.2 and 406.4 GHz spectra of **1** at 6.9 T and at 13.75 T, respectively, is a monomer contamination and is not present in a room-temperature spectrum (Figure S1). The molecular orientations at which respective transitions occur are marked with X, Y, and Z.

N(C) (bridge) direction and 11° from the Cu−Cu direction, and finally, the direction of the largest g component is 30° away from the longest Cu−N bond, roughly perpendicular to Cu−Cu (Figure S2). We label the direction of the smallest g component as "Z", while that of the intermediate g will be called "X". This facilitates the discussion of the zero-field splitting below. The spin Hamiltonian parameters for **1** and **3** are given in Table 4, along with those for $[Cu_2(\mu\text{-}Cl)(\mathbf{L}_m\text{*})_2](ClO_4)_3$[2a] and $[Cu_2(\mu\text{-}OH)(\mathbf{L}_m)_2](ClO_4)_3\cdot 2H_2O$.[2b] This Cl^-bridged complex is the best example of the d_{z^2} ground state in the entire copper-$\mathbf{L}_m/\mathbf{L}_m$* series, while the OH-bridged species exhibits the purest $d_{x^2-y^2}$ ground state. The zero-field splitting parameters for **1** and **3** are much smaller than those observed by us in the Cu-$\mathbf{L}_m/\mathbf{L}_m$* complexes bridged by halides or hydroxide.[2]

Sign of *D*. The exchange-related part of zfs can be extracted from the experimental D and E parameters of eq 4, and at this point their sign becomes important. These signs are not available from standard EPR because the resonance positions do not depend on them, but in high-field EPR the intensity pattern in the low-temperature spectra depends on the sign of D.[18] In an S = 1 spectrum, two "allowed" ΔM_S = 1 transitions are observed at any orientation of the magnetic field. At the "Z" orientation, the higher-field resonance in such a pair is stronger if D > 0 and weaker otherwise. The relation is opposite for the resonances at the "X" or "Y" orientations. The sign of D determination is relatively easy in cases of ferromagnetic or weakly antiferromagnetic complexes[18c,d] because spectra can be observed at very low temperatures where the effect becomes strong, up to completely freezing out either the lower-field or the higher-field transition. Complexes with a more pronounced antiferromagnetism require HFEPR measurements on large single crystals followed by the double integration of the spectra to determine the transition intensities.[18a,b] A sufficiently large crystal of **3** was grown and could be oriented in the EPR instrument so that the resonances were observed at the same magnetic field at which the Y features in the powder spectra

DOI: 10.1021/ic502485p
Inorg. Chem. 2015, 54, 1487−1500

appear (Figure 7). In an orientation perpendicular to the first one, resonances were observed very close to the Z features of

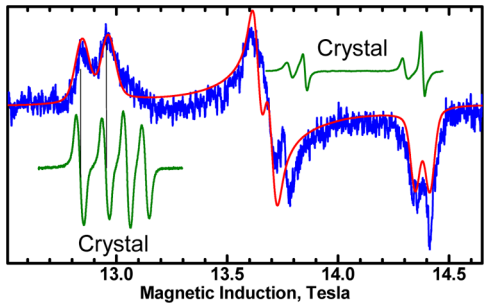

Figure 7. Blue: powder EPR spectrum of **3** (150 K, 406.4 GHz). Red: simulated with parameters from Table 4. Green: single-crystal spectra recorded at two mutually perpendicular orientations. At each orientation shown, two pairs of resonances appear due to the presence in the crystal lattice of two identical molecules, which are symmetry-related by a C_2 axis. These two molecules are oriented differently versus the magnetic field. The pair appearing at the lowest field corresponds almost perfectly to the "Y" features of the powder spectrum, as marked with the vertical lines. The highest-field pair is close to the "Z" features of the powder spectrum. See also Figure 8.

the powder spectra. The lowest temperature at which the intensity could be reliably measured was 30 K. The intensity pattern shown in Figure 8 proves the *positive* sign of D in **3** (see

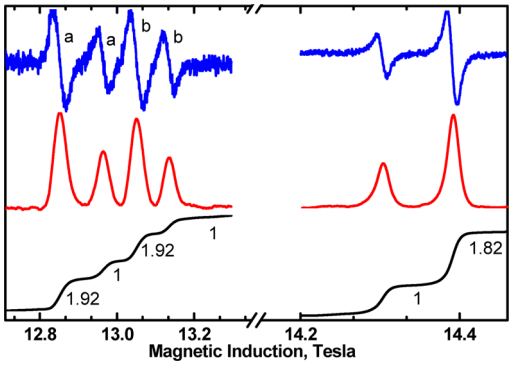

Figure 8. Single-crystal spectra of **3** recorded at 30 K and 406.4 GHz, at the same crystal orientations as in Figure 7, close to the Y orientation (left) and close to Z (right). Blue: original spectra (derivative of the absorption). Red: integrated spectra (absorption). Black: integrated absorption (intensity). The numbers are the relative intensities, with 1 assigned to the weaker line in a pair. Resonances due to the symmetry-related molecules "a" and "b" are so marked in the lower field spectra. In the higher-field spectra only the resonances due to the molecule close to the "Z" orientation are shown (compare to Figure 7). The intensity pattern is in agreement with a positive D parameter (see Figure 9).

Figure 9) and there is no reason to expect a different sign in **1**. The intensity ratio of the stronger to the weaker resonance in a pair, $R = (e^{h\nu/kT} - 1)/(1 - e^{-h\nu/kT})$[18a] is 1.91 at 30 K and 406.4 GHz, in a good agreement with the experimental ratios shown in Figure 8 (1.82–1.92). That ratio is 1.02 for the X-band frequency at 30 K, explaining the need of the HFEPR. One must be careful when reporting the sign of E because it is bound to the chosen system of coordinates. Using the parameters for **1** as an example, the parameter set g_x = 2.129, g_y = 2.142, g_z = 2.009, D = +0.0476 cm^{-1}, E = +0.0373 cm^{-1} is equivalent to a set g_x = 2.142, g_y = 2.129, g_z = 2.009, D =

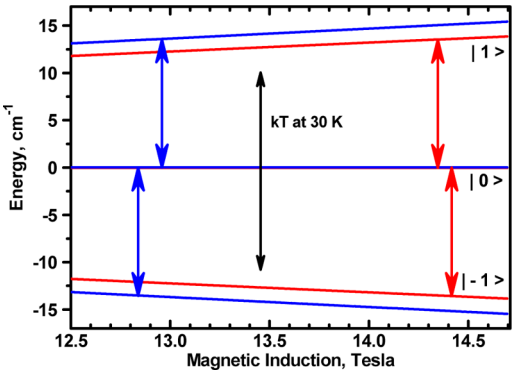

Figure 9. Energy of the $|M_S>$ states in the magnetic field calculated with the parameters of **3**. Blue: orientation Y; red: orientation Z. The blue and red arrows represent the 406.4 GHz microwave quantum energy (13.55 cm^{-1}) which is comparable to kT at 30 K (20.85 cm^{-1}). With positive D, the higher-field Z transition $|-1> \leftrightarrow |0>$ starts from the lowest energy state, while the lower-field Z transition $|0> \leftrightarrow |1>$ starting from the excited state will be suppressed at low temperature. The situation is opposite at the Y orientation. With a negative D these relations would be inverted and the high-field Z and low-field Y transitions would freeze out at low temperatures.

+0.0476 cm^{-1}, E = −0.0373 cm^{-1}, in which the coordinates X and Y were swapped.

With g_x and g_y labeled as in this paper, all E values in Table 4 are positive. Therefore, with the signs of the zfs parameters known the tensor components can be evaluated as shown in Table 5.

Table 5. Zero-Field Splitting Parameters D, E, and the zfs Tensor Components, in 10^{-4} cm^{-1}

	experimental[a]	dipole	exchange[b]	exchange[c]
	Data for **1** D = 476, E = 373			
D_{xx}	214	−155	369	121
D_{yy}	−532	86	−618	−866
D_{zz}	317	69	248	0
	Data for **3** D = 327, E = 308			
D_{xx}	199	−155	354	206
D_{yy}	−417	86	−503	−651
D_{zz}	218	70	148	0

[a]The experimental D_{ii} data were calculated from D and E observed at 150 K. [b]Difference $D_{ii} - D_{ii}^{dipole}$. [c]D_{zz}^{ex} component subtracted from D_{xx}^{ex}, D_{yy}^{ex} and D_{zz}^{ex}. This does not change the D^{ex} and E^{ex} values.

DFT Calculation of the Exchange Parameters (−J). "Broken symmetry"[19] DFT calculations were performed by using the software ORCA[20] to rationalize the magnitude of the exchange parameter J (often called exchange integral in literature). A self-consistent field (SCF) calculation is first performed for the maximum spin state of the dinuclear species. Next, a "broken symmetry" state is set up with the unpaired electron being spin-up on one metal and spin-down on the other, and another SCF calculation is carried out. The energies of the high-spin and broken symmetry states are finally used to estimate the $-J$ value (for Hamiltonian $\hat{\mathbf{H}} = -J\hat{\mathbf{S}}_1\hat{\mathbf{S}}_2$) based on the equation $-J = 2(\boldsymbol{E}_{HS}-\boldsymbol{E}_{BS})/(<\boldsymbol{S}^2>_{HS} - <\boldsymbol{S}^2>_{BS})$, where $\boldsymbol{E}_{HS}$ and $\boldsymbol{E}_{BS}$ are the energies of the high-spin (HS) and the broken-symmetry (BS) states and $<\boldsymbol{S}>^2$ are the expectation values of the spin-squared operator in the HS and BS states. Ahlrichs-type basis set TZVPP for copper(II) and all coordinated atoms

DOI: 10.1021/ic502485p
Inorg. Chem. 2015, 54, 1487−1500

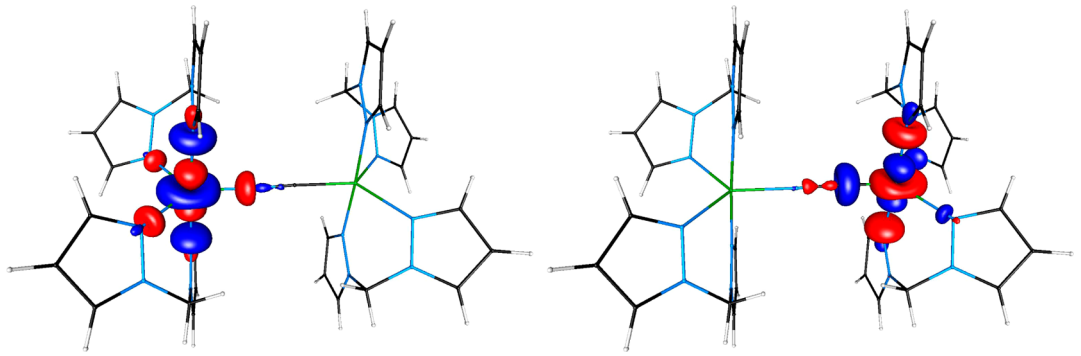

Figure 10. Copper(II) magnetic orbitals on the N-side (left) and on the C-side of the CN^- bridge calculated for **1**. The copper(II) unpaired electron delocalizes toward five coordinated ligand atoms.

and SVP for other atoms were used, combined with the B3LYP functional.[19,21] Ahlrichs polarization functions from basis H - Kr R and auxiliary bases from the TurboMole library were also used.[22]

The molecules were simplified by removal of the methyl groups on the pyrazolyl fragments (in $\mathbf{L}_m$*) as well as the benzene rings and placing hydrogen atoms at appropriate positions. All remaining atoms were retained at the positions determined by the X-ray structures. Compared to the halide and hydroxide bridges,[2] the CN^- and N_3^- bridges do not allow as much overlap of the magnetic orbitals (see Table 4) resulting in much smaller exchange interactions. The exchange coupling parameter $-J$ for **2** was strongly overestimated, while its magnitudes for **1** and **3** were closer to the experimental values, although the trend was not reproduced. The calculated $-J$ values were larger for the N_3^- bridge than for the CN^- bridge, and therefore this trend was reproduced. J obtained from the formula converting the energy difference between the high-spin and the broken symmetry state used in this paper is referred to in the literature as "spin-projected", and according to the ORCA manual, this should be good for strong exchange interactions. The "nonspin projected" formula results in 2 times smaller $-J$. There have been a lot of discussions among experts about which approach should be used; see for example ref 19. In our recent papers dealing with single-atom bridged copper(II) complexes of the ligands used here, we have always used the "spin-projected" J values, which were typically 30% larger than the experiment. If we had used the "nonprojected" method, our $-J$ values would have been underestimated by 35%. Similar relations were found in the present work. In both **1** and **3**, the calculated spin density on the bridging C atoms is larger than on the bridging N atoms. In **1** and **3**, as well as in $[Cu_2(\mu\text{-Cl})(\mathbf{L}_m^*)_2](ClO_4)_3$,[2a] (Table 4), the spin density is delocalized toward all five coordinated ligand atoms and is comparable but not equal on the two equatorial (nonbridging) nitrogen atoms (Figure 10). However, in **2** (Figure 11) and in $[Cu_2(\mu\text{-OH})(\mathbf{L}_m)_2](ClO_4)_3{\cdot}2H_2O$[2b] (Table 4), the spin density is delocalized toward only four ligands atoms. Also, the OH-bridged complex does not exhibit a very small g component, in contrast to **1**, **3**, and $[Cu_2(\mu\text{-Cl})(\mathbf{L}_m^*)_2](ClO_4)_3$. Unfortunately, there are no EPR data available for **2**. A correlation is observed in Table 4: smaller (i.e., closer to 2) g_z values correlate with larger geometric τ_5 parameter and with a more trigonal spin density distribution.

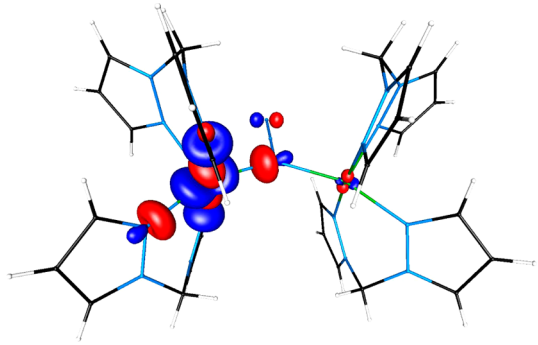

Figure 11. Magnetic orbital calculated for **2**. The copper(II) unpaired electron delocalizes toward only four coordinated nitrogen atoms. A magnetic orbital of identical shape exists on the other copper(II) atom (not shown).

DISCUSSION

We have successfully prepared the linearly bridged cyanide complexes $[Cu_2(\mu\text{-CN})(\mu\text{-}\mathbf{L})_2](ClO_4)_3{\cdot}x CH_3CN$ (**1**·3CH_3CN, $\mathbf{L} = \mathbf{L}_m$, **3**·2$CH_3CN$, $\mathbf{L} = \mathbf{L}_m$*). Although our earlier chemistry with nonbridged $[Ag_2(\mu\text{-}\mathbf{L}_m)_2]^{2+}$ complexes had indicated the Ag···Ag nonbonding distance is flexible over the range 4.83–5.31 Å,[23] these two CN^- bridged complexes are the first we have prepared with a diatomic bridge, leading to the largest separation (5.02–5.05 Å) of the two copper(II) cations in our extensive series of monoanionic bridged $[Cu_2(\mu\text{-X})(\mu\text{-}\mathbf{L})_2]^{3+}$ (X = F^-, Cl^-, Br^-, OH^- and $\mathbf{L} = \mathbf{L}_m$ or $\mathbf{L}_m$*) compounds.[2,8,24]

We have also prepared $[Cu_2(\mu\text{-}N_3)(\mu\text{-}\mathbf{L}_m)_2](BF_4)_3{\cdot}2.25CH_3CN$ (**2**·2.25CH_3CN), but in this case the copper(II) ions are bridged by a single nitrogen of the azide ligand. This complex, with end-on coordinated bridging azide, is the first with atoms other than hydrogen attached to the bridging atom. To accommodate this orientation of the bridging azide, the angle between the two mean planes of the phenylene spacers in the ligands is large at 33.37°, in comparison to analogous angles for $[Cu_2(\mu\text{-F})(\mu\text{-}\mathbf{L}_m)_2]^{3+}$ that vary between 0° and 2.32°.[8] This difference is shown in the space filling models in Figure 12a,b where the phenylene on the top in the pictures clearly rotates up in **2** (12a) to provide room for the end-on bridging azide. In addition, this geometry leads to the smallest Cu1–X–Cu2 bridging angle, 138.0°, found for all of the metallacycles of the type $[Cu_2(\mu\text{-X})(\mu\text{-}\mathbf{L})_2]^{3+}$.[2,8,24] We have previously shown in the case of $[Cu_2(\mu\text{-OH})(\mu\text{-}\mathbf{L}_m)_2](ClO_4)_3{\cdot}2H_2O$ that bending of the bridging Cu–X–Cu angle changes the geometry about the metals from trigonal bipyramidal toward square pyramidal geometry;[2b] the geometry around copper(II) in **2**·2.25CH_3CN

DOI: 10.1021/ic502485p
Inorg. Chem. 2015, 54, 1487–1500

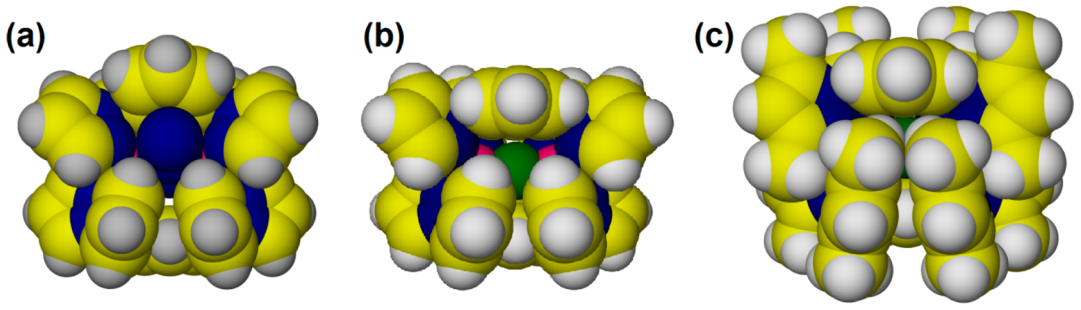

Figure 12. Space filling model of (a) $[Cu_2(\mu\text{-}N_3)(\mu\text{-}\mathbf{L}_m)_2]^{3+}$, (b) $[Cu_2(\mu\text{-}F)(\mu\text{-}\mathbf{L}_m)_2]^{3+}$, and (c) $[Cu_2(\mu\text{-}F)(\mu\text{-}\mathbf{L}_m{}^*)_2]^{3+}$.

can also be best described as square pyramidal. Interestingly, although the Cu1−N1−Cu2 angle is small in comparison to other $[Cu_2(\mu\text{-}X)(\mu\text{-}\mathbf{L})_2]^{3+}$ metallacycles, this angle is still large in comparison to other dinuclear complexes containing a single azide bridge.[5]

This unusual tilted orientation of one of the phenylene spacers in **2**·2.25CH_3CN supports the previously reported mechanism proposed for the dynamic behavior of $[Zn_2(\mu\text{-}OH)(\mu\text{-}\mathbf{L}_m)_2](ClO_4)_3$.[24a] This mechanism involves the 180° flip of the phenylene spacers along the $C_{methine}-C_{phenylene}$ bonds in a concerted mechanism with the Berry pseudorotation of the pyrazolyl rings at both zinc(II) sites—the two bis(pyrazolyl)-methane units coordinated to each zinc(II) rotate in opposite directions; the pivot ligand is the bridging hydroxide group. We termed these combined motions the "Columbia twist and flip" mechanism. Therefore, the structure of **2**·2.25CH_3CN is along the way to the intermediate in this proposed rearrangement process.

We attempted the synthesis of the azide bridged metallacycle with the $\mathbf{L}_m{}^*$ ligand starting from $[Cu_2(\mu\text{-}Cl)(\mu\text{-}\mathbf{L}_m{}^*)_2](ClO_4)_3$. In the presence of excess azide, the zigzag polymeric structure $[Cu_2(\mu\text{-}\mathbf{L}_m{}^*)(\mu\text{-}N_3)_2(N_3)_2]$ forms, similar to $[Cu(\mu\text{-}\mathbf{L}_p)(CH_3OH)](BF_4)_2\cdot(CH_3OH)_{0.62}$,[25] a complex of the analogous *para*-substituted ligand, where the bis(pyrazolyl)methane units are also on opposite sides of the phenylene spacer, the *anti*-conformation. The formation of the polymeric structure is not surprising in the light of the space filling model of the previously reported fluoride bridged metallacycles,[2,8] Figure 12b,c. In the metallacyclic system with $\mathbf{L}_m$, the ligand allows enough space for the end-on coordination of a bridging azide, Figure 12a. The $\mathbf{L}_m{}^*$ system blocks this position, as a result of the 3,5-methyl substitution of the pyrazolyl rings, and it is apparently not flexible enough to accommodate an end-to-end (μ-1,3) bridging azide.

Although still substantial, the antiferromagnetic super-exchange interactions of the cyanide bridged complexes **1** ($-J$ = 130 cm^{-1}) and **3** ($-J$ = 161 cm^{-1}) are, as expected for a diatomic bridge, lower than our previously reported single atom bridged complexes, where the lowest is $-J$ = 322 for $[Cu_2(\mu\text{-}F)(\mu\text{-}\mathbf{L}_m{}^*)_2](BF_4)_3$. These comparisons with this fluoride complex and $[Cu_2(\mu\text{-}Cl)(\mathbf{L}_m{}^*)_2](ClO_4)_3$ are particularly valid given the similar geometry, linear or nearly linear Cu−X−Cu angles. The EPR g parameters, supported by the DFT results, also indicate a similar d_{z^2} ground state. The closest comparison with other complexes containing a linear cyanide bridge is with $[\{Cu(L^1)\}_2(CN)](BF_4)_3$, where L^1 is a tetradentate N_4 ligand. In this case, the $-J$ = 104 cm^{-1} value is close to those reported here, although the geometry about the copper(II) ions and the orientation of the magnetic orbitals in the dinuclear unit in this complex is different.[6b]

In comparison, the antiferromagnetic interactions in complex **2**, with an end-on coordinated azide bridge and bent Cu−N−Cu angle of 138.0°, is larger ($-J$ = −223 cm^{-1}) than **1** and **3**, but still lower than our previously measured complexes. Our earlier results[2,8,24] and established theory[3] indicate that decreasing this bond angle lowers the antiferromagnetic interactions. In addition, as we have shown before for $[Cu_2(\mu\text{-}OH)(\mathbf{L}_m)_2](ClO_4)_3\cdot 2H_2O$, the DFT results are in agreement with the predominantly $d_{x^2-y^2}$ ground state for **2**. The "broken symmetry" calculations did not reproduce the trend of $-J$ being larger for **3** than for **1**. The calculations gave about the same $-J$ value for **3** and the molecule of **1** with the longer Cu···Cu distance (5.04 A), whereas a slightly larger $-J$ was obtained for the other molecule in **1** (Table 4).

The zfs parameters in a dinuclear copper(II) complex contain contributions due to the magnetic dipole−dipole interactions between the copper(II) ions plus a part associated with the anisotropic exchange interactions.[26] In matrix notation, we can write the zfs part of the spin Hamiltonian (4) as

$$\hat{H}_{zfs} = \hat{\mathbf{S}}\{D\}\hat{\mathbf{S}} \tag{5}$$

$$\{D\} = \{D\}^{dipole} + \{D\}^{ex} \tag{6}$$

The commonly used scalar D and E parameters of eq 4 are related to the diagonal elements of the respective $\{D\}$ tensors (that is the dipolar, or exchange, or the total one) by

$$D = (2D_{zz} - D_{xx} - D_{yy})/2,\ E = (D_{xx} - D_{yy})/2 \tag{7}$$

The dipolar contribution can be reasonably estimated by using the point dipole model. In our coordinate system in which the X axis is close to the Cu···Cu direction, we have

$$D_{xx}{}^{dipole} = -g_x{}^2\mu_B{}^2/R^3{}_{Cu-Cu}$$

$$D_{yy}{}^{dipole} = g_y{}^2\mu_B{}^2/2R^3{}_{Cu-Cu}$$

$$D_{zz}{}^{dipole} = g_z{}^2\mu_B{}^2/2R^3{}_{Cu-Cu} \tag{8}$$

The exchange-related contributions to zero-field splitting can be extracted from the experimental parameters, since our high field studies have also been able to definitively show that the signs of D and E are positive. These results are shown in Table 5.

The scalar parameters D^{ex} and E^{ex} (see eq 7) for **1** are equal to 372 × 10^{-4} cm^{-1} and 493 × 10^{-4} cm^{-1}, respectively, and for **3** they are 222 × 10^{-4} cm^{-1} and 428 × 10^{-4} cm^{-1}, respectively. Note that D^{ex} and E^{ex} do not obey the convention $|E| < |D|/3$ because of choice of the system of coordinates in which the Z axis corresponds to the smallest g component. The convention can always be re-established by renaming the axes of

DOI: 10.1021/ic502485p
Inorg. Chem. 2015, 54, 1487−1500

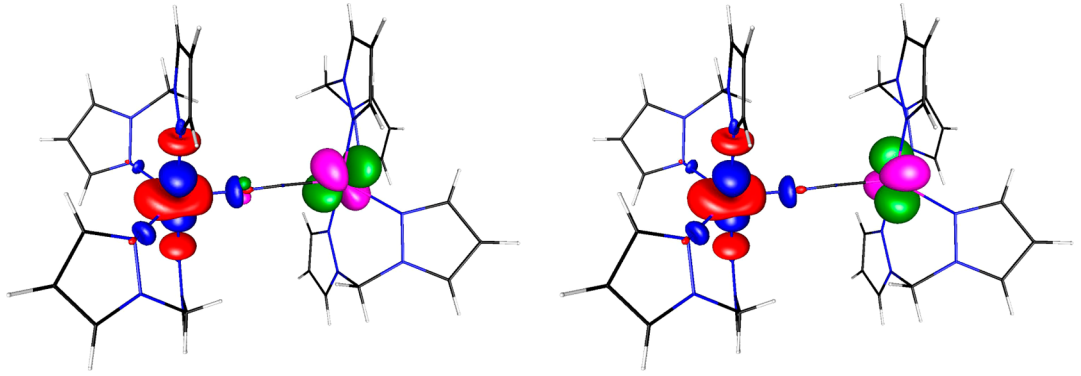

Figure 13. Zero-field splitting is affected by the exchange interactions between the ground state d_{z^2} of one copper ion with either a d_{xz} state of another (left) or with d_{yz} (right). The exchange integral $J_{z^2,yz}$ is expected to be very different from $J_{z^2,xz}$ because of the orbital arrangement.

coordinates, as described in the Supporting Information published with ref 2c.

The exchange related contribution to zfs is caused by the spin−orbit coupling mediated mixing of the excited states of the dinuclear system to its ground state.[1b,18,26,27] The excited states under question are such in which one of the copper(II) ions is in its ground state (d_{z^2}) while the other copper(II) is in one of the excited states.[1b,18,26,27] Moreover, an excited state can only contribute if a nonzero matrix element of the **L** operator exists between that excited state and the ground state. In the present case, only the excited states d_{xz} and d_{yz} need to be considered, and the exchange-related contributions to D and E parameters depend on the sum and difference, respectively of two terms, $\lambda^2 J_{z^2,yz}/(\Delta E_{z^2,yz})^2$ and $\lambda^2 J_{z^2,xz}/(\Delta E_{z^2,xz})^2$ in which the expressions $J_{z^2,yz}$ and $J_{z^2,xz}$ are the exchange integrals between the d_{z^2} orbital of one copper ion and d_{xz} or d_{yz} of another. $\lambda = -828$ cm^{-1} is the spin−orbit coupling constant for copper(II), and $\Delta E_{z^2,xz}$, $\Delta E_{z^2,yz}$ are the energy differences between the ground and excited orbitals. The former of these terms determines the magnitude of the anisotropic exchange-related zero-field splitting tensor component D^{ex}_{xx} and the later one relates to D^{ex}_{yy}, while the D^{ex}_{zz} component must be 0, as the $\mathbf{L_z}$ operator has no matrix elements with any other d orbital. The X axis is the Cu···Cu direction, and the Z axis is the trigonal bipyramid axis. The formulas for D^{ex} and E^{ex} were derived[2b] following a method described in ref 25a:

$$D^{ex}\ \frac{3}{4}\frac{\lambda^2 J_{z^2,yz}}{\Delta E^2_{z^2,yz}} + \frac{3}{4}\frac{\lambda^2 J_{z^2,xz}}{\Delta E^2_{z^2,xz}}$$

$$E^{ex}\ -\frac{3}{4}\frac{\lambda^2 J_{z^2,yz}}{\Delta E^2_{z^2,yz}} + \frac{3}{4}\frac{\lambda^2 J_{z^2,xz}}{\Delta E^2_{z^2,xz}} \qquad (9)$$

Or using the tensor components,

$$D^{ex}_{xx} = -\frac{3}{2}\frac{\lambda^2 J_{z^2,yz}}{\Delta E^2_{z^2,yz}}$$

$$D^{ex}_{yy} = -\frac{3}{2}\frac{\lambda^2 J_{z^2,xz}}{\Delta E^2_{z^2,xz}}$$

$$D^{ex}_{zz} = 0 \qquad (9a)$$

As a result of the orbital arrangements presented in Figure 13, the interactions between the d_{z^2} orbital of one ion and d_{xz} of another ion is expected to be different from the $d_{z^2} - d_{yz}$ interaction, resulting in large E^{ex} in this type of compound.[2] In Table 5, the experimental zfs tensor components were calculated from the experimental D and E parameters using eq 7. The dipole−dipole contribution was then subtracted to obtain the exchange part resulting in the D_{xx}^{ex}, D_{yy}^{ex}, and D_{zz}^{ex} shown in the column before the last in Table 5. The D_{zz}^{ex} component in that column is not zero because a D tensor determined from EPR is always traceless. Adding a common component to each of the three D_{ii} does not change the D and E parameters of spin Hamiltonian (4) according to eq 7, and therefore no change in the simulated EPR spectra will result. Since we expect D_{zz}^{ex} be equal to 0, we subtract D_{zz}^{ex} from each of the D_{ii}^{ex} to obtain the last column in Table 5. The ratios $\lambda/(\Delta E_{z^2,yz})$ and $\lambda/(\Delta E_{z^2,xz})$ which are present in eq 9 also appear in the g factor theory for copper(II). For the d_{z^2} ground state we have

$$g_x = 2.0023 - \frac{6\lambda}{\Delta E(d_{z^2,xz})}$$

$$g_y = 2.0023 - \frac{6\lambda}{\Delta E(d_{z^2,xz})}$$

$$g_z = 2.0023 \qquad (10)$$

The ratios $\lambda/(\Delta E_{z^2,yz})$ and $\lambda/(\Delta E_{z^2,xz})$ calculated from the experimental g values (Table 4) are 0.02 and 0.04, respectively. Going back to eq 9a and the last column of Table 5, one can estimate for **3** $J_{z^2,yz} = -(2/3)\ D_{xx}^{ex}/(\lambda\Delta E_{z^2,yz})^2 = -34 \times 10^{-4}$ cm^{-1}, $J_{z^2,xz} = -(2/3)\ D_{yy}^{ex}/(\lambda\Delta E_{z^2,xz})^2 = 27 \times 10^{-4}$ cm^{-1}, while for **1** $J_{z^2,yz} = -20 \times 10^{-4}$ cm^{-1}, $J_{z^2,xz} = 36 \times 10^{-4}$ cm^{-1} are obtained. The quality of these J values depends on the quality of the dipolar contribution estimation. The point-dipole approximation was used in Table 5, but the dipolar interactions may be strongly affected by the electron delocalization effects. For example, in the classical copper acetate the point-dipole method produced[18a] $D^{dip} = -0.171$ cm^{-1}, while -0.118 cm^{-1} was calculated using the wave function.[27a] In our CN^--bridged molecules, the spin densities of two copper ions are delocalized onto the bridging C and N atoms. Those spin density fractions are in close proximity and contribute strongly to D^{dip}. Such an effect has indeed been observed in a biradical system,[28] in which the point dipole D^{dip} value was by a factor of 2.5 too small compared to the quantum-chemical value, the latter being in agreement with experiment.[28] We have thus applied the ORCA software[20−22] to calculate D^{dip}. It produced the dipolar

DOI: 10.1021/ic502485p
Inorg. Chem. 2015, 54, 1487−1500

tensor components (in 10^{-4} cm^{-1}) $D_{xx}^{dip} = -185$, $D_{yy}^{dip} = 103$, $D_{zz}^{dip} = 82$, while the point-dipole values are −155, 86, and 69, respectively (Table 5). Using the new dipolar tensor components in calculations above causes only small changes in $J_{z^2,yz}$ and $J_{z^2,xz}$, the former remaining negative and the latter positive for both **1** and **3**. Although very different $J_{z^2,yz}$ and $J_{z^2,xz}$, were expected, the negative (antiferromagnetic) character of the former is a surprise as the d_{z^2} orbital of one Cu appears to have net zero overlap with the d_{xz} orbital of another Cu (Figure 13). The zero-field splitting in **1** is substantially larger than in **3**. Because of the structural closeness, the dipolar contribution to zfs must be similar. Further, the similarity of the g_x and g_y magnitudes in **1** and **3** indicates that the terms $(\lambda\Delta E_{z^2,yz})^2$, $(\lambda/\Delta E_{z^2,xz})^2$ of eq 9 should be similar in both complexes, and it must be the differences in the exchange integrals $J_{z^2,yz}$ and $J_{z^2,xz}$ that make zfs in **1** and **3** different. Confirming this, as well as the signs of these two exchange integrals, would require complicated ab initio calculations like those in ref 27a,d, which are better left to the experts in the field.

Complexes **1** and **3** have an inversion center according to the X-ray structure, but this must be understood as a statistical average, since the CN^- bridge is asymmetric. A single molecule has no inversion center and the antisymmetric exchange (Dzialoshinskii–Moriya) interactions[29] are possible. Although no difficulties in simulating the EPR spectra of **1** and **3** were encountered when using just spin Hamiltonian (4), it can be shown that the antisymmetric exchange is very difficult to detect in a dinuclear copper(II) complex, while it has dramatic effects in other systems, like trinuclear copper complexes with a triangular arrangement.[29b−e] The DM interaction adds to a spin Hamiltonian a term containing the cross-product of $\hat{\mathbf{S}}_1$ and $\hat{\mathbf{S}}_2$:

$$\hat{H}_{DM} = \boldsymbol{d}\cdot(\hat{\mathbf{S}}_1 \times \hat{\mathbf{S}}_2) \quad (11)$$

where $\boldsymbol{d}$ is a vector quantity (the Dzialoshinkii–Moriya vector).

The idealized structures of our CN-bridged complexes **1** and **3** would have a *xz* mirror plane passing through both copper atoms and the nitrogen atoms in the apexes of the trigonal bipyramids. According to the Moriya rules,[29a,e] this implies a nonzero d_y component of $\boldsymbol{d}$. Figure 14 shows the magnetic susceptibility calculated with the parameters of **3** (with no monomer impurity) and with the same parameters plus $d_y = 40$ cm^{-1}, i.e., 25% of the isotropic exchange. It is seen that even this massive DM interaction affects only the lowest temperature data, as it produces a TIP-like contribution to the magnetic susceptibility (of 66×10^{-6} cgs emu per 1 copper atom), which results from mixing of the $S = 0$ and $S = 1$ states.[29e] Moreover, the EPR spectra appear to offer little help. A massive DM interaction would be seen in the EPR spectra while still being undetectable in the magnetic susceptibility, but a smaller one, of the order of a few cm^{-1}, can be compensated by changing the *D* and *E* parameters. Figure 15 shows a spectrum simulated with the parameters of **1** ($D = 0.0476$ cm^{-1}, $E = 0.0373$ cm^{-1}) as well as an alternative simulation in which only the dipolar part of the zero-field splitting was used, $D^{dipole} = 0.0103$ cm^{-1}, $E^{dipole} = -0.0120$ cm^{-1}, and the "missing part" of *D* and *E* was compensated by the DM component $d_y = 6.7$ cm^{-1}. This compensation works for any microwave frequency, including the X-Band (see the Supporting Information). The surprising finding of an antiferromagnetic $J_{z^2,yz}$ above may be thus an artifact caused by the contamination of the zero-field splitting parameters by the antisymmetric exchange.

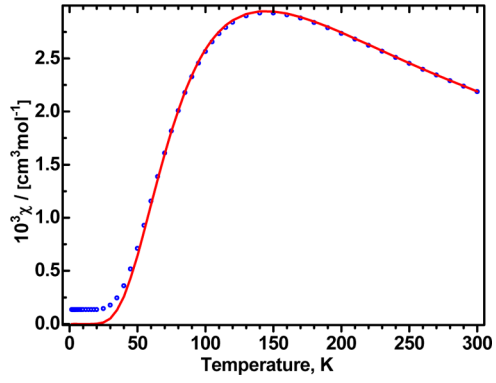

Figure 14. Effect of the Dzialoshinskii–Moriya interaction on the magnetic susceptibility. Red line: calculated with parameters of **3** without DM exchange; blue circles: calculated with $d_y = 40$ cm^{-1} and other parameters unchanged.

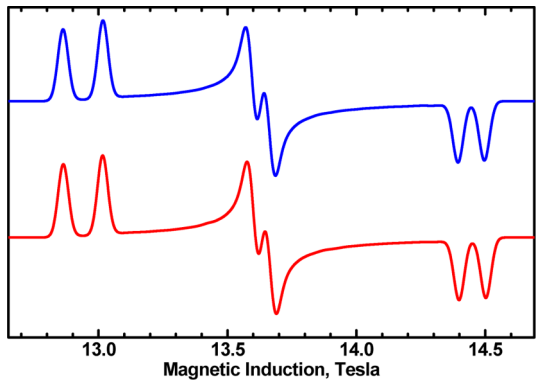

Figure 15. Top: EPR spectrum (406.4 GHz, 30 K) simulated with parameters of **1** and no antisymmetric exchange. Bottom: simulation with $d_y = 6.7$ cm^{-1} and only the dipolar part of the zero-field splitting ($D^{dipole} = 0.0103$ cm^{-1}, $E^{dipole} = -0.0120$ cm^{-1} (from parameters in Table 5).

CONCLUSIONS

We show here that the dinuclear metallacyclic system is flexible enough to accommodate not only one, but two bridging atoms by the preparation of the cyanide bridged compounds $[Cu_2(\mu\text{-}CN)(\mu\text{-}\mathbf{L})_2](ClO_4)_3$, with both $\mathbf{L}_m$ and $\mathbf{L}_m$* ligands. Attempts to prepare a complex with three bridging atoms between the metals, an end-to-end coordinated azide, led instead to a metallacycle $[Cu_2(\mu\text{-}N_3)(\mu\text{-}\mathbf{L}_m)_2](ClO_4)_3$, with end-on coordination of N_3^-. Because the bulkier $\mathbf{L}_m$* ligand blocks the end-on coordination mode of N_3^-, a polymeric structure rather than a metallacycle forms in this case. The I^- ion reduces copper(II) prohibiting the isolation of an iodide bridged metallacycle.

The linearly bridged cyanide complexes **1** and **3** show relatively strong antiferromagnetic interactions, but these interactions are weaker than our previously reported single atom bridged $[Cu_2(\mu\text{-}X)(\mu\text{-}\mathbf{L}_m)_2]^{3+}$ (X = F^-, Cl^-, OH^-, Br^-) complexes. High field EPR studies have determined that the g_x, g_y, and g_z values in these two cyanide bridged complexes are very different from each other, and one of them is very close to 2, indicating the d_{z^2} ground state of the copper(II) ions.[2] We have also shown that the sign of the *D* and *E* parameters are positive and calculated the contributions to them due to the dipole–dipole and the anisotropic exchange interactions. The zero-field splitting is clearly dominated by the latter

DOI: 10.1021/ic502485p
Inorg. Chem. 2015, 54, 1487−1500

interactions. The end-on coordinated azide complex **2** shows antiferromagnetic interactions intermediate between the cyanide complexes and our previously reported complexes bridged by a single atom, likely because the Cu−N−Cu angle is the smallest in the series, and the magnetic orbitals have predominantly $d_{x^2-y^2}$ character.

■ ASSOCIATED CONTENT

Ⓢ Supporting Information

X-ray crystallographic files in CIF format, high field, X and Q-Band EPR spectra of **1** and **3**, directional components of *g*, simulations using the Moriya term. This material is available free of charge via the Internet at http://pubs.acs.org.

■ AUTHOR INFORMATION

Corresponding Authors

*(D.L.R.) Tel: 803-777-2587. Fax: 803-777-9521. E-mail reger@mailbox.sc.edu.

*(A.O.) E-mail ozarowsk@magnet.fsu.edu.

Notes

The authors declare no competing financial interest.

■ ACKNOWLEDGMENTS

The authors acknowledge with thanks the financial support of the National Science Foundation through Grant CHE-1011736. The high-field EPR spectra were recorded at the NHMFL, which is funded by the NSF through the Cooperative Agreement No. DMR-1157490, the State of Florida, and the DOE. This work was partly financed by a subsidy for statutory activity from Ministry of Science and Higher Education of the Republic of Poland for Faculty of Chemistry, University of Wroclaw.

■ REFERENCES

(1) (a) Kahn, O. *Inorg. Chim. Acta* **1982**, *62*, 3−14. (b) Bleaney, B.; Bowers, K. D. *Proc. R. Soc. London, A* **1952**, *214*, 451−465. (c) Lee, S. C.; Holm, R. H. *Inorg. Chem.* **1993**, *32*, 4745−4753. (d) Koval, I. A.; van der Schilden, K.; Schuitema, A. M.; Gamez, P.; Belle, C.; Pierre, J.; Lüken, M.; Krebs, B.; Roubeau, O.; Reedijk, J. *Inorg. Chem.* **2005**, *44*, 4372−4382 and references therein. (e) Marino, N.; Armentano, D.; De Munno, G.; Cano, J.; Lloret, F.; Julve, M. *Inorg. Chem.* **2012**, *51*, 4323−4334. (f) Kahn, O. In *Molecular Magnetism*; VCH Publishers Inc.: New York, 1993. (g) Saito, T.; Yasuda, N.; Nishihara, S.; Yamanaka, S.; Kitagawa, Y.; Kawakami, T.; Okumura, M.; Yamaguchi, K. *Chem. Phys. Lett.* **2011**, *505*, 11−15. (h) Noro, S.; Akutagawa, T.; Nakamura, T. *Chem. Commun.* **2010**, *46*, 4619−4621.

(2) (a) Reger, D. L.; Pascui, A. E.; Smith, M. D.; Jezierska, J.; Ozarowski, A. *Inorg. Chem.* **2012**, *51*, 7966−7968. (b) Reger, D. L.; Pascui, A. E.; Smith, M. D.; Jezierska, J.; Ozarowski, A. *Inorg. Chem.* **2012**, *51*, 11820−11836. (c) Reger, D. L.; Pascui, A. E.; Foley, E. A.; Smith, M. D.; Jezierska, J.; Ozarowski, A. *Inorg. Chem.* **2014**, *53*, 1975−1988.

(3) Hay, J. P.; Thibeault, J. C.; Hoffmann, R. *J. Am. Chem. Soc.* **1975**, *97*, 4884−4899.

(4) (a) Adhikary, C.; Koner, S. *Coord. Chem. Rev.* **2010**, *254*, 2933−2958. (b) Escuer, A.; Aromí, G. *Eur. J. Inorg. Chem.* **2006**, 4721−4736. (c) Cabrero, J.; de Graaf, C.; Bordas, E.; Caballol, R.; Malrieu, J.-P. *Chem.—Eur. J.* **2003**, *9*, 2307−2315. (d) Banerjee, A.; Singh, R.; Colacio, E.; Rajak, K. K. *Eur. J. Inorg. Chem.* **2009**, 277−284. (e) Ravikumar, I.; Suresh, E.; Ghosh, P. *Inorg. Chem.* **2006**, *45*, 10046−10048. (f) Amendola, C.; Fabbrizzi, L.; Mangano, C.; Pallavicini, P.; Michele, Z. *Inorg. Chim. Acta* **2002**, *337*, 70−74. (g) Xie, Y.; Liu, Q.; Jiang, H.; Du, C.; Xu, X.; Yu, M.; Zhu, Y. *New J. Chem.* **2002**, *26*, 176−179. (h) Benzekri, A.; Dubourdeaux, P.; Latour, J.-M.; Laugier, J.; Rey, P. *Inorg. Chem.* **1988**, *27*, 3710−3716. (i) Chou, J.-L.; Horng, D.-N.; Chyn, J.-P.; Lee, K.-M.; Urbach, F. L.; Lee, G.-H.; Tsai, H.-L. *Inorg. Chem. Commun.* **1999**, 392−395. (j) Matsumoto, K.; Ooi, S.; Mori, W.; Nakao, Y. *J. Chem. Soc., Dalton Trans.* **1990**, 3117−3121. (k) Benzekri, A.; Dubourdeaux, P.; Latour, J.-M.; Rey, P.; Laugier, J. *J. Chem. Soc., Dalton Trans.* **1991**, 3359−3365. (l) Chattopadhyay, P.; Sabnam Banu, K.; Banerjee, A.; Ribas, J.; Majee, A.; Nethaji, M.; Das, D. *J. Mol. Struct.* **2007**, *833*, 13−22. (m) Tandon, S. S.; Thompson, L. K.; Manuel, M. E.; Bidson, J. M. *Inorg. Chem.* **1994**, *33*, 5555−5570. (n) Thompson, L. K.; Tandon, S. S.; Manuel, M. E. *Inorg. Chem.* **1995**, *34*, 2356−2366. (o) Ichiro, M.; Ikuhiko, U.; Nobuhiro, M.; Sigeo, K.; Naohide, M.; Machiko, K.; Makoto, T.; Kumiko, H.; Masahiro, M. *J. Chem. Soc., Dalton Trans.* **1990**, 2763−2769. (p) Plieger, P. G.; Downard, A. J.; Moubaraki, B.; Murray, K. S.; Brooker, S. *Dalton Trans.* **2004**, 2157−2165. (q) McLachlan, G. A.; Fallon, G. D.; Martin, R. L.; Moubaraki, B.; Murray, K. S.; Spiccia, L. *Inorg. Chem.* **1994**, *33*, 4663−4668. (r) Shen, Z.; Zuo, J.-L.; Gao, S.; Song, Y.; Che, C.-M.; Fun, H.-K.; You, X.-Z. *Angew. Chem., Int. Ed.* **2000**, *39*, 3633−3635. (s) Hall, G. R.; Duggan, D. M.; Hendrickson, D. N. *Inorg. Chem.* **1975**, *14*, 1956−1964.

(5) (a) Harding, C. J.; Mabbs, F. E.; MacInnes, E. J. L.; McKee, V.; Nelson, J. *J. Chem. Soc., Dalton Trans.* **1996**, 3227−3230. (b) Naiya, S.; Biswas, C.; Drew, M. G. B.; Gómez-García, C. J.; Clemente-Juan, J. M.; Ghosh, A. *Inorg. Chem.* **2010**, *49*, 6616−6627. (c) Lin, X.-J.; Shen, Z.; Song, Y.; Xu, J.-H.; Li, Y.-Z.; You, X.-Z. *Inorg. Chim. Acta* **2005**, *358*, 1963−1969.

(6) (a) Jungst, R.; Stucky, G. *Inorg. Chem.* **1974**, *13*, 2404−2408. (b) Atanasov, M.; Comba, P.; Hanson, G. R.; Hausberg, S.; Helmle, S.; Wadepohl, H. *Inorg. Chem.* **2011**, *50*, 6890−6901. (c) Bond, A. D.; Derossi, S.; Harding, C. J.; McInnes, E. J. L.; McKee, V.; McKenzie, C. J.; Nelson, J.; Wolowska, J. *Dalton Trans.* **2005**, 2403−2409. (d) Parker, R. J.; Spiccia, L.; Moubaraki, B.; Murray, K. S.; Skelton, B. W.; White, A. H. *Inorg. Chim. Acta* **2000**, *300−302*, 922−931. (e) Flay, M.-L.; Vahrenkamp, H. *Eur. J. Inorg. Chem.* **2003**, 1719−1726. (f) Rodríguez-Fortea, A.; Alemany, P.; Alvarez, S.; Ruiz, E.; Scuiller, A.; Decroix, C.; Marvaud, V.; Vaissermann, J.; Verdaguer, M.; Rosenman, I.; Julve, M. *Inorg. Chem.* **2001**, *40*, 5868−5877. (g) Lu, T.; Zhuang, X.; Li, Y.; Chen, S. *J. Am. Chem. Soc.* **2004**, *126*, 4760−4761. (h) Lim, B. S.; Holm, R. H. *Inorg. Chem.* **1998**, *37*, 4898−4908. (i) Scott, M. J.; Lee, S. C.; Holm, R. H. *Inorg. Chem.* **1994**, *33*, 4651−4662. (j) Xu, F.; Huang, W.; You, X.-Z. *J. Chem. Soc., Dalton Trans.* **2010**, *39*, 10652−10658. (k) Thaler, F.; Hubbard, C. D.; Heinemann, F. W.; van Eldik, R.; Schindler, S.; Fábián, I.; Dittler-Kingemann, A. M.; Hahn, F. E.; Orvig, C. *Inorg. Chem.* **1998**, *37*, 4022−4029. (l) Gomila, A.; Douziech, B.; Cosquer, N.; Poul, N. L.; Michaud, F.; Gomez-Garcia, C. J.; Mest, Y. L.; Conan, F. *Inorg. Chim. Acta* **2014**, *411*, 67−76.

(7) (a) Chaudhuri, B.; Winter, M.; Flörke, U.; Haubt, H. J. *Inorg. Chim. Acta* **1995**, *232*, 125−130. (b) Lobana, T. S.; Khanna, S.; Butcher, R. J. *J. Chem. Soc., Dalton Trans.* **2012**, *41*, 4845−4851. (c) Zhou, X.-P.; Li, D.; Zheng, S.-L.; Zhang, X.; Wu, T. *Inorg. Chem.* **2006**, *45*, 7119−7125. (d) Johnson, J. E.; Jacobson, R. A. *J. Chem. . Soc. Dalton Trans.* **1973**, 580−584.

(8) Reger, D. L.; Foley, E. A.; Watson, R. P.; Pellechia, P. J.; Smith, M. D. *Inorg. Chem.* **2009**, *48*, 10658−10669.

(9) Hassan, A. K.; Pardi, L. A.; Krzystek, J.; Sienkiewicz, A.; Goy, P.; Rohrer, M.; Brunel, L.-C. *J. Magn. Reson.* **2000**, *142*, 300−312.

(10) (a) O'Connor, C. J. *Prog. Inorg. Chem.* **1982**, *29*, 203−283. (b) Bain, G. A.; Berry, J. F. *J. Chem. Educ.* **2008**, *85*, 532−536.

(11) *SMART*, Version 5.631, *SAINT+*, Version 6.45, and *SADABS*, Version 2.10; Bruker Analytical X-ray Systems, Inc.: Madison, Wisconsin, USA, 2003.

(12) Sheldrick, G. M. *Acta Crystallogr.* **2008**, *A64*, 112−122.

(13) Dolomanov, O. V.; Bourhis, L. J.; Gildea, R. J.; Howard, J. A. K.; Puschmann, H. *J. Appl. Crystallogr.* **2009**, *42*, 339−341.

(14) (a) LePage, Y. *J. Appl. Crystallogr.* **1987**, *20*, 264−269. (b) Spek, A. L. *J. Appl. Crystallogr.* **1988**, *21*, 578−579. (c) Spek, A. L. *Acta Crystallogr., Sect. A* **1990**, *46*, C34−C37. (d) Spek, A. L. *PLATON, A Multipurpose Crystallographic Tool*; Utrecht University, Utrecht: The Netherlands, 1998.

DOI: 10.1021/ic502485p
Inorg. Chem. 2015, 54, 1487−1500

(15) The τ_5 values in Table 1 were calculated according to: $\tau_5 = ((\beta - \alpha)/60°)$, where α and β are the two largest angles measured around the metal centers. Addison, A. W.; Rao, T. N.; Reedijk, J.; Van Rijn, J.; Verschoor, G. C. *J. Chem. Soc., Dalton Trans.* **1984**, 1349−1356.
(16) (a) Bersuker, I. B. In *The Jahn−Teller Effect*; University Press: Cambridge, UK, 2006. (b) Harrison, D.; Kennedy, D.; Hathaway, B. *Inorg. Nucl. Chem. Lett.* **1981**, *17*, 87−90. (c) Kepert, D. L. In *Inorganic Chemistry Concepts*; Springer-Verlag: New York, 1982; Vol. *6*, p 36.
(17) Comba, P.; Lampeka, Y. D.; Prikhod'ko, A. I.; Rajaraman, G. *Inorg. Chem.* **2006**, *45*, 3632−3638.
(18) (a) Ozarowski, A. *Inorg. Chem.* **2008**, *47*, 9760−9762. (b) Ozarowski, A.; Szymanska, I. B.; Muziol, T.; Jezierska, J. *J. Am. Chem. Soc.* **2009**, *131*, 10279−10292. (c) Sharma, R. P.; Saini, A.; Monga, D.; Venugopalan, P.; Jezierska, J. *New J. Chem.* **2014**, *38*, 437−447. (d) Semenaka, V. V.; Nesterova, O. V.; Kokozay, V. N.; Dyakonenko, V. V.; Zubatyuk, R. I.; Shishkin, O. V.; Boca, R.; Jezierska, J.; Ozarowski, A. *Inorg. Chem.* **2010**, *49*, 5460−5471.
(19) Ruiz, E.; Cano, J.; Alvarez, S.; Alemany, P. J. *Comp. Chem.* **1999**, *20*, 1391−1400. Onofrio, N.; Mouesca, J. M. *Inorg. Chem.* **2011**, *50*, 5577−5886.
(20) (a) Neese, F. *ORCA - An ab initio, Density Functional and Semiempirical Program Package*, Version 2.9.1; Surf Sara: Amsterdam, 2012. (b) Neese, F. *Comput. Mol. Sci.* **2012**, *2*, 73−78.
(21) (a) Becke, D. A. *Phys. Rev. A* **1988**, *38*, 3098−3100. (b) Perdew, J. P. *Phys. Rev. B* **1986**, *33*, 8822−8824. (c) Perdew, J. P. *Phys. Rev. B* **1986**, *34*, 7406−7406. (d) Kendall, R. A.; Früchtl, H. A. *Theor. Chem. Acc.* **1997**, *97*, 158−163.
(22) (a) Schaefer, A.; Horn, H.; Ahlrichs, R. *J. Chem. Phys.* **1992**, *97*, 2571−2577. (b) Ahlrichs, R. et al., unpublished results. The Ahlrichs auxiliary basis sets were obtained from the TurboMole basis set library under ftp.chemie.uni-karlsruhe.de/pub/jbasen.
(23) Reger, D. L.; Watson, R. P.; Smith, P. J. *Inorg. Chem.* **2006**, *45*, 10077−10087.
(24) (a) Reger, D. L.; Pascui, A. E.; Pellechia, P. J.; Smith, M. D. *Inorg. Chem.* **2013**, *52*, 11638−11649. (b) Reger, D. L.; Pascui, A. E.; Pellechia, P. J.; Ozarowski, A. *Inorg. Chem.* **2013**, *52*, 12741−12748.
(25) Reger, D. L.; Pascui, A. E.; Smith, M. D. *Eur. J. Inorg. Chem.* **2012**, *29*, 4593−4604.
(26) (a) Abragam, A.; Bleaney, B. *Electron Paramagnetic Resonance of Transition Ions*; Clarendon Press: London, 1970. (b) Bencini, A.; Gatteschi, D. *EPR of Exchange Coupled Systems*; Springer Verlag: Berlin, 1990.
(27) (a) Maurice, R.; Sivalingam, K.; Ganyushin, D.; Guihery, N.; de Graaf, C.; Neese, F. *Inorg. Chem.* **2011**, *50*, 6229−6236. (b) Gribnau, M. C. M.; Keijzers, C. P. *Inorg. Chem.* **1987**, *26*, 3413−3414. (c) Ross, P. K.; Allendorf, M. D.; Solomon, E. I. *J. Am. Chem. Soc.* **1989**, *111*, 4009−4021. (d) Singh, S. K.; Rajaraman, G. *Chem.—Eur. J.* **2014**, *20*, 5214−5218.
(28) Riplinger, C.; Kao, J. P. Y.; Rosen, G. M.; Kathirvelu, V.; Eaton, G. R.; Eaton, S. S.; Kutateladze, A.; Neese, F. *J. Am. Chem. Soc.* **2009**, *131*, 10092−10106.
(29) (a) Moriya, T. *Phys. Rev.* **1960**, *120*, 91−98. (b) Yoon, J.; Solomon, E. I. *Coord. Chem. Rev.* **2007**, *251*, 379−400. (c) Ferrer, S.; Lloret, F.; Pardo, E.; Clemente-Juan, J. M.; Liu- González, M.; García-Granda, S. *Inorg. Chem.* **2012**, *51*, 985−1001. (d) Vasylevskyy, S. I.; Senchyk, G. A.; Lysenko, A. B.; Rusanov, E. B.; Chernega, A. N.; Jezierska, J.; Krautscheid, A.; Domasevitch, K. V.; Ozarowski, A. *Inorg. Chem.* **2014**, *53*, 3642−3654. (e) Boča, R.; Herchel, R. *Coord. Chem. Rev.* **2010**, *254*, 2973−3025.

DOI: 10.1021/ic502485p
Inorg. Chem. 2015, 54, 1487−1500